BBB recovery after stroke by self-replenishing E-pericytes transdifferentiated from local endothelial cells.

Tingbo Li[1],Jiaqi Tu[2], Qingzhu Gao[2], Xuzhao Li[2], Zhu Zhu[2], Yuxiao Jin[2], Yiyi Zhang[2], Jiongfang Xie[3], Peiran Zhu[4], Bingrui, Zhao[2], Jie-Min Jia*[2, 5, 6, 7]

[1]College of Life Sciences, Zhejiang University, Hangzhou, Zhejiang, 310058, China.

[2]Laboratory of Neurovascular Biology, School of Life Sciences, Westlake University, Hangzhou, 310024, China.

[3]Key Laboratory of Structural Biology of Zhejiang Province, School of Life Sciences, Westlake University, Hangzhou, Zhejiang, 310024, China.

[4]School of Materials Science and Engineering, Zhejiang University, Hangzhou, China.

[5] Westlake Laboratory of Life Sciences and Biomedicine, Hangzhou, 310024, China

[6]Key Laboratory of Growth Regulation and Translational Research of Zhejiang Province, School of Life Sciences, Westlake University, Hangzhou, 310024, China.

[7]Institute of Basic Medical Sciences, Westlake Institute for Advanced Study, Hangzhou, 310024, China.

*Correspondence: jiajiemin@westlake.edu.cn

Ischemic stroke causes a significant amount of cell death, including pericytes. Chronic perfused phase of ischemic stroke, the number of pericytes increases, and limited research has been explorated on the reasons for the recovery of pericytes. By genetic tracing, we identified ECs undergoing cell-fate changing, through TGFb-pSMAD3-EndoMT pathway transdifferentiation, into pericytes (E-pericytes). Some of the migrating E-pericytes induced by stroke are derived from detached ECs. The E-pericytes can integrate into vasculature again, suggesting ischemic brains can recycle ECs from unfunctional vessels to replenish lost pericytes as an innate self-maintenance program sustaining repair phenomena. We also found E-pericytes promotes BBB restoration, increases angiogenesis and restores cerebral blood flow(CBF), resulting more neurons survive and accelerating behavioral rehabilitation.

Stroke kills millions each year and no effective treatment is available so far[1]. Brains possess an intrinsic, limited self-repair capacity[2, 3], e.g. spontaneous angiogenesis after stroke. However, understanding the definitive spontaneous repairing processes is largely incomplete. ECs form vascular tubes, while pericytes encircle the endothelial tube. The observation that more pericytes die faster than ECs may explain neurodegeneration exacerbation and brain self-recovery hindering after stroke because pericytes are a type of pericytess known to be critical for the blood-brain barrier and cerebral blood flow[4-6]. However, little is known about cellular sources for pericyte regeneration in the adult ischemic brain while it has been well documented that the cephalic neural crest gives rise to pericytes in all blood vessels of the face and forebrain during embryonic development[7, 8]. Many capillaries collapse after stroke, however, the

43 fate of endothelial cells from these unfunctional vessels to be recycled or to die is
44 unclear. Recently, Yu et al. have demonstrated that pericytes can be differentiated
45 locally from a subgroup of ECs in multiple tissues under homeostasis[9]. However, the
46 case in brains with or without ischemia remains unknown. Identification of origin cells for
47 regenerated pericytes and EC's fate in the ischemic brain is of importance for
48 enhancing endogenous capacity to repair a stroke-damaged brain.

49 First, we found that using flow cytometric analysis revealed that after 2 days of
50 reperfusion, close to 50% of pericytes were lost, while endothelial cells accounted for
51 less than 20% (Fig. 1a). With the prolonged reperfusion time, the numbers of pericytes
52 and endothelial cells both show recovery, with the percentage of pericyte recovery
53 exceeding 40% and the percentage of endothelial cell recovery approaching 10% at
54 RP34D, comparion to RP2D(Fig. 1b-d). This indicates that in the chronic phase of
55 ischemic reperfusion, there are ways for both endothelial cells and pericytes to increase
56 the cell number. In ischemic stroke mice continuously treated with EdU by
57 intraperitoneal injection every day for 34 days, we observed the presence of EdU^+
58 pericytes(Fig. 1e-f). After statistical analysis(Fig. 1g), it was found that EdU^+ pericytes
59 accounted for less 20% of the total pericytes, suggesting that over 20% of pericytes
60 may not be generated through self-proliferation, comparison with flow analysis results.
61 Could these non-EdU^+ pericytes originate from the transformation of endothelial cells?

62 To test if cerebral ECs differentiate into pericytes during adult angiogenesis as do
63 those in the mammary gland, skin, and retina[9], we employed a cell fate tracing system
64 by crossing EC-specific DNA recombinase driver line *Cdh5-CreERT2*[10] with triple EGFP
65 reporter (Ai47)[11] or tdTomato reporter (Ai14) (The Jackson Laboratory) (Fig. 2a). ECs

66 and their potential progeny cells are permanently labeled by EGFP or tdTomato
67 fluorescent proteins once tamoxifen (TAM) is provided(Extended Data Fig.2a). At the
68 same time, When tamoxifen was not given, there was no EGFP signal(Extended Data
69 Fig.2a-b). Upon long-term TAM exposure (Fig. 2b), although some of these EGFP$^+$ ECs
70 in skin tissue change their fates into EGFP$^+$ pericytes[9], brain EGFP$^+$ ECs, however,
71 seemed never (Fig. 2c-e). all EGFP$^+$ cells remained expressing multiple classical
72 endothelial markers, such as ERG, GluT1 and VE-cadherin, despite up to a two-year
73 tracing (Extended Data Fig.2c-f). Consistent with previous reports[9, 10, 12], these
74 fluorescent proteins were restricted in ECs but not in any other types of brain cells
75 short-term after TAM exposure (4 - 7 days, Extended Data Fig. 2g-m). At the same time，
76 ECs and their potential progeny cells are never labeled by pericyte markers: PDGFRβ,
77 NG2, CD13, Caldesmon and α-SMA (Fig.2f-h;Extended Data Fig.2n-q). Together, these
78 results demonstrated unlike in the peripheral system and retina, cerebral ECs are not
79 the cellular source for pericytes in adult brains under homeostasis.

80 Ischemic stroke, modeled by middle cerebral artery occlusion (MCAO, Extended
81 Data Fig.2r-t), induced cerebral ECs detaching from vessels, gradually losing EC
82 markers, basal membrane protein, and undergoing drastic morphological changes such
83 as losing hollow structure and growing multiple processes from cell soma (Fig. 2i;
84 Extended Data Fig.2u-v). This finding suggested that ECs might undergo cell fate
85 changing in response to ischemia attack. Thus, we referred to this subgroup of EGFP$^+$
86 cells as 'EGFP$^+$ non-EC cells'. TAM was delivered to 1.5-month-old mice and then at
87 least two weeks later we performed MCAO surgery (Fig. 2b), aiming to ensure no extra
88 residual TAM. After 2-hour MCAO, sutures were withdrawn, permitting various periods

89 of reperfusion, ranging from 8 all the way through 514 days (RP2D to RP514D)
90 (Extended Data Fig.2w-z). These EGFP$^+$ non-EC cells can be found anywhere possible
91 in the ischemic region, showing no regional specificity (Extended Data Fig. 2a1).
92 According to whether having secondary processes, we classified EGFP$^+$ non-EC cells
93 into two types: type I, short, and fewer primary processes, no secondary processes
94 (Extended Data Fig. b1,d1-e1); type II, longer and more primary branches with
95 secondary ones (Extended Data Fig. b1,d1-e1), while their cell bodies were comparable
96 in shape and size (Extended Data Fig. f1).

97 We found that the prevalence of these two types of cells switched when reperfusion
98 period prolonged. (Extended Data Fig. c1). This morphological switching suggests type I
99 becoming type II gradually. The prevalence of EGPF$^+$ non-EC cells started to rise at
100 RP8D, peaked by RP52D, and finally declined back to a low level (Extended Data Fig.z).
101 This curve suggested that these transformed avascular EGFP$^+$ non-EC cells may die or
102 be recruited back to vessels, becoming vascular cells again. We termed this possibility
103 a recycling process. Furthermore, FACS analysis (RP34D) revealed an EGFP$^+$ but
104 CD31 negative population (EGFP$^+$ non-EC cells, Fig. 2j). These EGFP$^+$ transformed
105 cells accounted for ~1.2% of total EGFP$^+$ cells which included ECs and non-EC cells
106 (Fig. 2k).

107 *Cdh5-CreERT2* may label a small portion of neutrophils and monocytes in the bone
108 marrow and circulation[12] (Extended Data Fig. 3 a-b), which are known to enter brain
109 parenchyma shortly after stroke onset but dies out[13]. To discriminate whether
110 parenchyma EGFP$^+$ non-EC cells are derived from EGFP$^+$ bone marrow cells in
111 *Cdh5CreERT2;Ai47* mice, we introduced a viral expression system restricted to ECs

112 preventing EGFP expression in hematopoietic cells (Extended Data Fig. 3c-e).
113 Specifically, we injected cranially the Cre-dependent *AAV-CAG-DIO-EGFP* virus to
114 *Cdh5-CreERT2* single-positive mice that do not carry *Ai47* or *Ai14* reporter (Extended
115 Data Fig. 3c), resulting in high labeling specificity to ECs (Extended Data Fig. 3f-g).
116 Once again, we found $EGFP^+$ ECs transforming into $EGFP^+$ non-EC cells after stroke
117 (Extended Data Fig. 3h). Notably, some of these cells extended their long processes
118 and enwrapped capillaries, reminiscent of pericyte characteristics (Extended Data Fig.
119 3h). Independent radiation experiment was implemented to exclude the same possibility,
120 we replaced *Cdh5CreERT2;Ai47* mice's bone marrow with wild type ones (Extended
121 Data Fig. 3i-j). Despite the depletion of $EGFP^+$ bone marrow cells under this
122 circumstance (Extended Data Fig. 3i-j), we still found comparable $EGFP^+$ non-EC cells
123 in ischemic regions (Extended Data Fig. 3k-n), demonstrating that $EGFP^+$ immune cells
124 were not the cell source of $EGFP^+$ non-EC cells in parenchyma. These results together
125 indicate that a small proportion (1.2%) of ECs detached from vessels in the parenchyma,
126 lost EC features, and changed their cellular identity after subjecting them to ischemia
127 insult.

128 To assess whether these $EGFP^+$ non-EC cells are derived from vascular stem
129 endothelial cells as reported previously[9] which involves cell proliferation, we traced cell
130 division events by injecting EdU for consecutive 34 days. No single $EGFP^+$ non-ECs
131 were found to be EdU positive after examining 15 brain slices from two mice (Fig. 2l-m).
132 similarly, neither Ki67 signals were found (Extended Data Fig. 4a-b). Thus, we
133 concluded these $EGFP^+$ non-EC cells may not be progenies of stem cells, suggesting

134 that a transdifferentiation process may be required. Fortunately, EGFP+ non-EC cells
135 appear at the classical pericyte location (Fig. 2n-o).

136 By employing a list of cell type markers, we identified that 90% of EGPF$^+$ non-EC
137 cells were pericytes (namely, E-pericytes) as they were positive for typical pericyte
138 markers of CD13(90%), PDGFRβ(75%), and NG2 (Fig. 2p-s;Extended Data Fig. 4c), as
139 well as that they were negative for all of the markers of immature and mature neurons
140 (doublecortin and NeuN), astrocytes (GFAP), CNS macrophages (Iba1, CD68, and
141 F4/80), immuce cells (CD45), and smooth muscle cells (α-SMA) (Extended Data Fig.
142 4d-f). The cell identity of the rest 10% of EGFP+ non-EC cells remained unknown (Fig.
143 3g) though as these cells were not labeled by any cell markers that we used.
144 Furthermore, more than a quarter of EGFP$^+$ pericytes were recruited back to vessels
145 (Fig. 2p-q,v), suggesting ECs were fully recycled not only by expressing pericyte
146 markers but also by locating the right anatomical position. A transformed tdTomato$^+$
147 non-ECs (here, Ai14 reporter was used instead of Ai47) that were also tracked by *AAV-*
148 *DIO-EGFP* virus exhibited one process attaching a capillary while the other did not
149 (Extended Data Fig. 4g), implying capturing a recruiting moment. It has been repeatedly
150 reported that pericytes detach from vessels after stroke[14]. We found actually a third of
151 these avascular, migrating pericytes were derived from ECs (Fig. 2v). Further analysis
152 revealed that 23.3% of total vascular pericytes were EGFP$^+$ (Fig. 2t), suggesting ECs
153 are a fair contributor cell source for pericyte regeneration. The virus-tracked ECs also
154 can generate pericytes, coinciding with results from genetic tracing (Extended Data Fig.
155 4h-i). Meanwhile, we also employed other methods to specifically label endothelial cells
156 to validate the E-pericytes phenomenon. Tie2Dre;Msfd2aXER mice were used for

157 specific tracing of endothelial cells in the brain[15]. Firstly, we verified their specificity
158 using endothelial cell markers(Extended Data Fig. 4j-k). After MCAO/RP34D, we still
159 observed the presence of $CD13^+$E-periytes (Extended Data Fig. 4n). We also use AAV-
160 Bi30-Cre virus which can be traced ECs in mouse brain[16]. AAV-Bi30-Cre virus was
161 injected via the eye socket in Ai47 mice and we still observed the presence of $CD13^+$E-
162 periytes (Extended Data Fig. 4i-m,o).These results together demonstrate that after
163 ischemic stroke, ECs transdifferentiated into E-pericytes, likely capable of integrating
164 back into the cerebral vasculature.

165 To further verify the identified $EGFP^+$&$CD31^-$ cells as pericyte, we analyzed the
166 transcriptomic characteristics of $EGFP^+$&$CD31^-$ cells. First, we obtained $EGFP^+$&$CD31^-$
167 cells (MCAO:2H/RP34D) using flow cytometric sorting. The flow cytometric gating
168 strategy was $CD45^-$&$Viability^+EGFP^+$&$CD31^-$ cells(Fig. 3a). The sorted cells from each
169 group were as follows: non-stroke endothelial cells (Con-ECs), ipsilateral stroke
170 endothelial cells (Ipsi-ECs), and $EGFP^+$&$CD31^-$ cells derived from the ipsilateral side
171 (Ipsi-ETCs). After library construction, sequencing was performed. PCA analysis
172 revealed that Con-ECs and Ipsi-ECs had similar principal component relationships
173 because they were both endothelial cells, although they were derived from different
174 environments of the endothelial cells (non-ischemia and ischemia brain tissue,
175 respectively)(Fig. 3b). On the other hand, Ipsi-ETCs showed greater dissimilarity to the
176 principal component relationships of Con-ECs and Ipsi-ECs(Fig. 3b). This result
177 remained consistent different batches, suggesting significant differences in the
178 transcriptomes between Ipsi-ETCs and the endothelial cells represented by Con-ECs
179 and Ipsi-ECs, even though Ipsi-ETCs were derived from $EGPF^+$ normal endothelial cells.

180 Heatmap analysis of all genes indicated that the transcriptomes of Con-ECs and Ipsi-
181 ECs were more similar and clustered closely, despite some differences caused by the
182 ischemic environment(Fig. 3c). In contrast, the transcriptome differences between Ipsi-
183 ETCs and Con-ECs/Ipsi-ECs were more pronounced, and Ipsi-ETCs from different
184 batches tended to cluster together(Fig. 3c). These findings indicated significant
185 differences between the transcriptomes of $CD45^{-}$&$Viability^{+}EGFP^{+}$&$CD31^{-}$ cells and
186 endothelial cells. Subsequently, we analyzed the expression of endothelial cell marker
187 proteins among different groups. We found that the expression of endothelial cell
188 markers genes in Ipsi-ETCs significantly decreased compared to Con-ECs and Ipsi-ECs,
189 and this decrease was observed across most endothelial cell marker genes(Fig. 3d).
190 Con-ECs and Ipsi-ECs still expressed numerous endothelial cell marker genes,
191 although differences existed between them(Fig. 3d). Additionally, we analyzed the
192 expression of pericyte-related transcriptomes genes among different groups. We
193 observed a significant increase in the expression of pericyte marker genes in Ipsi-ETCs,
194 particularly in specific transcription factors(Fig. 3e), membrane proteins(Fig. 3f), and
195 ligand proteins associated with pericytes(Fig. 3g). Conversely, the expression of
196 pericyte-related marker genes was lower in Con-ECs and Ipsi-ECs, suggesting that the
197 transcriptome of Ipsi-ETCs exhibited characteristics of pericyte cell transcriptomes
198 genes. Furthermore, volcano plot analysis of ETCs/Ipsi-ECs identified differentially
199 expressed genes with statistical significance(Fig. 3h). GO enrichment analysis revealed
200 that the Ipsi-ETCs group was more enriched in functionally related genes associated
201 with fate conversion, such as high expression of genes involved in cell differentiation,
202 cell movement, cell migration, and endothelial cell migration, as well as low expression

203 of genes related to endothelial cell junction genes(Fig. 3i). These findings were
204 consistent with the observations in ischemic brain slices, where 2/3 of Ipsi-ETCs
205 detached from the blood vessels. Additionally, KEGG pathway enrichment analysis
206 revealed that genes related to metabolic pathways were upregulated, while genes
207 related to endothelial cell tight junctions were downregulated(Fig. 3j). GSEA analysis
208 showed that genes associated with endothelial cell features, such as endothelial cell
209 differentiation, cell junctions, and cell apoptosis, were downregulated(Fig. 3k-m), while
210 genes associated with glucose metabolism pathways and ATP production through
211 aerobic respiration were upregulated(Fig. 3n-p). It is known that endothelial cells have
212 fewer mitochondria and primarily produce ATP through glycolysis, whereas Ipsi-ETCs
213 showed a significant increase in genes related to glucose metabolism, as well as genes
214 involved in ATP production. This suggests that important genes in the metabolic
215 pathway of glucose metabolism are altered in Ipsi-ETCs. These results collectively
216 indicate that Ipsi-ETCs exhibit significant differences in the genomic profile compared to
217 endothelial cells and show transcriptional characteristics of pericyte cells, providing
218 further evidence from the transcriptome analysis that $EGFP^{+}$ non-EC cells are E-
219 pericytes.

220 The above experiments have demonstrated that the ischemic microenvironment after
221 stroke promotes the transdifferentiation of endothelial cells into E-pericytes. Next, we
222 attempted to explore the mechanism by which endothelial cells transform into E-pericyte.
223 In 2016, Yu QC et al. reported the identification of endothelial cells expressing Protein C
224 Receptor (Procr) in breast tissue, which possess characteristics of vascular endothelial
225 stem cells (VESCs). Procr+ VESCs have strong proliferative abilities in vitro and also

226 participate in vascular remodeling in live animals. Lineage tracing studies have found
227 that this group of cells can transform into pericytes during breast development, and the
228 transcriptome of Procr+ VESCs exhibits characteristics of Endothelial-to-Mesenchymal
229 Transition (EndoMT) and Epithelial-to-Mesenchymal Transition (EMTs), suggesting that
230 the transformation of endothelial cells into pericytes in breast development may occur
231 through EndoMT[9]. We found that after ischemic stroke, the expression of EndoMT
232 marker proteins in ischemic regions of endothelial cells was significantly increased.
233 Specifically, at MCAO:2H/RP2D, the expression of phosphorylated SMAD3 (an impor-
234 tant kinase in the TGF β pathway-activated by phosphorylation) as an EndoMT marker
235 protein increased in the ischemic region(Fig. 4a-c). Furthermore, MCAO:2H/RP8D, the
236 expression of p-SMAD3 in ECs also increased in the ischemic region(Fig. 4a-c).
237 However, MCAO:2H/RP34D, endothelial cells almost did not express p-SMAD3 as an
238 EndoMT marker protein, and E-pericytes cells also almost did not express p-
239 SMAD3(Fig. 4a-c). At 8 days post ischemia, we also observed two adjacent $EFGP^+$
240 cells on the same blood vessel, one cell exhibiting $CD31^+$&p-$SMAD3^-$, still maintaining
241 endothelial cell characteristics, while the other cell exhibiting $CD31^-$& p-$SMAD3^+$,
242 indicating that after p-SMAD3 is expressed in some endothelial cells, the characteristic
243 molecule CD31 is reduced or not expressed(Fig. 4d), indicating successfully catching
244 cells undergoing transition on time. At 2 days post ischemia, the expression of KLF4 (an
245 important transcription factor in the EndoMT pathway) as an EndoMT marker protein in
246 the ischemic region of endothelial cells increased(Extended Data Fig.5a-c). At 8 days
247 post ischemia, the expression of KLF4 in the ischemic region of endothelial cells
248 decreased, and at 34 days post ischemia, the expression of KLF4 as an EndoMT

249 marker protein in endothelial cells further decreased, and E-pericytes cells almost did
250 not express KLF4(Extended Data Fig.5a-c). At 2 days post ischemia, the expression of
251 α-SMA (an important marker protein in EndoMT) in the ischemic region of endothelial
252 cells increased(Extended Data Fig.5d-f). At 8 days post ischemia, the expression of α-
253 SMA as an EndoMT marker protein in the ischemic region of endothelial cells
254 decreased, and at 34 days post ischemia, the expression of α-SMA in endothelial cells
255 also decreased, and E-pericytes cells almost did not express α-SMA (Extended Data
256 Fig.5d-f). Furthermore, cytoplasmic flow cytometry demonstrated that at 2 days post
257 ischemia, the expression of α-SMA in endothelial cells increased, reaching 1.6% of the
258 proportion of endothelial cells in the ischemic region, which is close to the proportion of
259 E-pericytes cells (1.2%) in the ischemic region(Extended Data Fig.5g-h). Next, we
260 investigate the potential molecular signaling pathway that might mediate this E-pericytes.
261 Since TGFβ signaling is well documented for cell fate changing including the endothelial
262 mesenchymal transition (EndMT) process, a newly recognized type of
263 transdifferentiation[17,18]. Therefore, we injected LY364947 and SB431542, TGFβRI
264 inhibitors when MCAO was performed, followed by additional daily injections for
265 consecutive 2 days of reperfusion. The expression of p-SMA3, KLF4 and α-SMA
266 protein in the ischemic region of endothelial cells decreased in TGFβRI inhibitors
267 group(Extended Data Fig.5i-j), and cytoplasmic flow cytometry demonstrated that at 2
268 days post ischemia, the expression of α-SMA in endothelial cells decrease(Extended
269 Data Fig.5k-i). For consecutive 34 days of reperfusion, We found significantly fewer
270 $EGFP^+$ non-EC cells appeared overall(Extended Data Fig.5m-n). FACS analysis further
271 confirmed this conclusion quantitively (Extended Data Fig.5o-p). The specific knockout

272 of the *Tgfbr2* gene in endothelial cells also resulted in a decrease of EndoMT markers
273 (p-SMAD3, KLF4, and α-SMA) at the RP2D(Fig. 4e-h), along with a decrease in the
274 number of E-pericytes(Fig. 4i-l). These results strongly suggested that TGFβ-pSMAD3-
275 EndoMT signaling involved in E-pericytes is centrally important. Together, under
276 ischemic conditions, ECs exploited TGFβ signaling to transform ECs into pericytes
277 during reperfusion to replenish the shrunk pericyte pool occurring in the acute ischemia
278 period.

279 Pericyte-deficient mouse mutants shows that pericyte deficiency increases the
280 permeability of the BBB to water and a range of low-molecular-mass and high-
281 molecular-mass tracers[19,20]. Therefore, we speculate that E-pericytes participate in the
282 recovery of the blood-brain barrier (BBB) during the chronic recovery period after
283 ischemic stroke. E-pericytes can return to the blood vessels and perform functions such
284 as maintaining BBB integrity, reducing the entry of harmful substances into the brain,
285 promoting angiogenesis, increasing capillary density, and improving blood supply to
286 facilitate the recovery of neurons and other cells, ultimately promoting self-repair.

287 Studies in mouse models showed that, in the absence of key TGFβ receptors,
288 angiogenesis stalls in the yolk sac at an early stage with fatal consequences[21]. The
289 effect of endothelial cell-specific knockout of Tgfbr2 on blood vessel development and
290 endothelial function in adult mice is unknown. Firstly, we found that specific knockout of
291 the Tgfbr2 gene in endothelial cells does not affect the function of BBB (Extended Data
292 Fig.6a). At the same time, it also did not affect the expression of the BBB-related protein
293 ZO-1(Extended Data Fig.6b-c). Furthermore, under electron microscopy, the basement
294 membrane remains intact(Extended Data Fig.6d-e), and the tight connections between

295 endothelial cells are normal(Extended Data Fig.6f). There is also no obvisous
296 occurrence of transcytosis phenomena caused by BBB disruption in the endothelial
297 cells(Extended Data Fig.6g). This indicates that knocking out Tgfbr2 in adult mice does
298 not affect the BBB function of vascular endothelial cells.

299 At different reperfusion time points, reducing E-pericytes by specifically knocking out
300 Tgfbr2 in endothelial cells can aggravate the chronic BBB leakage. In the group with
301 Tgfbr2 knocked out specifically in endothelial cells, the BBB function was significantly
302 impaired when the reperfusion time exceeded 7 days(Fig.5a-b). When reperfused timely
303 for 118 days, it still showed low Evan blue leakage(Fig.5a-b). This suggests that
304 reducing E-pericytes through specific knockout of Tgfbr2 in endothelial cells can affect
305 the recovery of chronic BBB during reperfusion.

306 We observed a decrease in $NeuN^+$ neurons after ischemic stroke, with a more
307 significant decrease in the reducing E-pericytes mouse group(Fig.5c-d). Additionally, we
308 quantified the number of $CD13^+$ pericytes in the ischemic area and found a significant
309 decrease in pericyte density(Fig.5e-f), which is consistent with previous studies. In the
310 reducing E-pericytes group, the reduction in pericyte density was more significant
311 (Fig.5e-f). The ratio of endothelial cells to pericytes on the blood vessels was also
312 significantly lower than the normal group(Fig.5g). We measured the length of $CD31^+$
313 endothelial cells in the ischemic area and found a decrease in length(Fig.5h-i), and flow
314 cytometry analysis showed a more pronounced decrease in $CD31^+$ endothelial cells in
315 the reducing E-pericytes mouse group, indicating decreased angiogenesis(Fig.5j-k).
316 Furthermore, laser speckle contrast analysis revealed poorer blood flow recovery in the
317 reducing E-pericytes mouse group(Fig.5i-m), as well as more pronounced brain atrophy

318 (Fig.5n-o). This suggests that in the E-pericytes mouse group, reduced E-periytes lead
319 to impaired blood flow recovery during reperfusion, resulting in more cell death and
320 more significant brain atrophy. To test animal locomotion function, $Tgfbr2^{fl/fl}$, $EC^{Tgfbr2fl/+}$,
321 and $EC^{Tgfbr2fl/fl}$ mice groups were subjected to 2 hours of ischemia followed by 34 days of
322 reperfusion, and behavioral tests were conducted at different time points (0D, 1 day, 3
323 days, 7 days, 14 days, 21 days, and 34 days of reperfusion). Animal locomotion function
324 tests related to motor function, including pole test, beam walking test, turning test, and
325 adhesive removal test, were performed. Compared to the $Tgfbr2^{+/+}$ group, mice in
326 $EC^{Tgfbr2fl/fl}$ group showed shorter pole test duration and had statistically significant
327 differences starting from 21 days of reperfusion(Fig.5p); mice in $EC^{Tgfbr2fl/fl}$ group spent
328 less time on the beam and had statistically significant differences starting from 21 days
329 of reperfusion(Fig.5q); mice in $EC^{Tgfbr2fl/fl}$ group exhibited more pronounced differences
330 in the turning test compared to the normal values, with statistically significant
331 differences starting from 14 days of reperfusion(Fig.5r); mice in $EC^{Tgfbr2fl/fl}$ group were
332 less likely to remove the adhesive tape from their forepaws in the adhesive removal test,
333 with statistically significant differences starting from 14 days of reperfusion(Fig.5s).
334 These results indicate that the motor recovery ability of $EC^{Tgfbr2fl/fl}$ group is poorer, which
335 may be associated with reducng E-periytes.

336 Overall, using mouse genetic tracing tools combined with virus infection,
337 pharmacology and genetically modified mice, we demonstrated adult ischemic brains
338 spontaneously repair microvasculatures by regenerating new pericytes that are
339 transformed from ECs after detaching from vessels. Distinct from the previous findings
340 in peripheral organs in which a small group of endothelial stem cells $Procr^{+}$ ECs

differentiate into pericytes during adult angiogenesis under homeostasis[9], ECs do not become pericytes in normal brains but transdifferentiate into pericytes without cell division. The death rate is dozens of times higher in pericytes than in ECs within 24 hours after a transient focal ischemia[4], suggesting abundant capillaries become damaged by being naked. What is the fate of these naked capillaries made up by ECs? The present study suggests that these naked vessels may release ECs, some of which may not die but rather be recycled and repurposed by the ischemic brain. By observing type I simpler form switching to type II more complex $EGFP^+$ E-pericytes (Extended Data Fig.2c1) and the medium stage of the transformed $EGFP^+$ E-pericytes (Extended Data Fig. 4g), we extrapolate them likely being recruited and serve as building blocks to repair the existing damaged vasculatures. This could be an efficient system to reuse brain cells that have lost their original functions. Further studies are required to live imaging the whole dynamic process during reperfusion periods.

Identifying new cellular sources for pericyte replenishment is important not only for stroke but also for many other either acute or chronic brain injuries. This study may suggest a novel therapy for generating EC-derived pericyte without involving stemness which has long been a concern for tumorigenesis.

Methods

Experimental design. Transgenic Cdh5CreERT2 transgenic mice[10] cross with reporter mice *Ai47 ($EGFP^{f/f}$) reporter* or *Ai14 ($tdTomato^{f/f}$) reporter mice*. Thus, ECs are labeled in green or red initially. TAM was delivered when mice were 1.5 months old (6 weeks), i. e. genetic tracing started. After waiting for 2 weeks, MCAO was performed. After a 2-hour occlusion, reperfusion began. Contralateral sides of the ischemic brain were used

364 as objects for homeostasis conditions, except for the time point of tracing 4 days. Thus,
365 it was traced for 22 days in the PR8D mice (N = 3 mice), 1.6 months in RP34D (N = 27
366 mice), 2.8 months in RP71D (N = 3 mice), 14 months in RP408D (N = X mice), 8.2
367 months in RP232D (N = 3 mice), 14 months in RP408D (N = 2 mice),17.6 months in
368 RP51D mice (N = 2 mice). The tracing time point of 1.6 months (RP34D) was the most
369 frequently examined. FACS and immunohistochemistry were the major two techniques
370 used for cell identity confirmation.

371 **Animal care and tissue dissection.**

372 All animal experiments were carried out in accordance with protocols approved by the
373 Institutional Animal Care and Use Committee (IACUC) at the School of Life Sciences,
374 Westlake University. Wild-type C57BL6/J mice were purchased from the Laboratory
375 Animal Resources Center of Westlake University. Cdh5CreERT2 mice were a gift from
376 Le-Ming Zheng (Peking University). Gt(ROSA)26Sor$^{tm47(CAG\text{-}EGFP^{*})Hze}$ (Ai47) was share by
377 Zilong Qiu (ION). We crossed Cdh5Cre-ERT2 mice to Ai47 mice to generate
378 Cdh5CreERT2:Ai47 mice. Standard chow and water were provided to mice *ad libitum*.
379 Four mice were housed in each cage. All animals were housed in a standard animal
380 room with a 12/12-hour light/dark cycle at 25 °C. Both male and female mice were used
381 in this study. Mice were anaesthetized by intraperitoneal injection pentobarbital sodium
382 (100 mg/kg), and brain dissection was performed immediately for FACS experiments or
383 cardiac PFA perfusion was performed for immunohistochemistry experiment. After
384 fixation, brains were dissected and kept in 4% PFA for additional 4 hours and then
385 transferred to PBS until further processing.

386 **MCAO**

387 Adult mice were anesthetized with pentobarbital sodium (100 mg/kg) and body
388 temperature was maintained during surgery with a heating pad. A midline neck incision
389 was made, the right common carotid artery was carefully separated from the vagus
390 nerve, and the artery was ligated using a 5.0-string. A second knot was made on the left
391 external carotid artery. The right internal carotid artery (ICA) was isolated, and a knot
392 was left loose with a 5.0-string. This knot was not tightened until the intraluminal
393 insertion was done. A small hole was cut on the common carotid artery before it was
394 bifurcated to the external carotid artery and ICA. A silicon-coated monofilament (tip
395 diameter = 230 μm, Doccol Corporation, 602256PK5Re) was gently advanced into the
396 ICA until it stopped at the origin of the MCA in the circle of Willis. The third knot on the
397 ICA was closed to fix the filament in position. During MCA occlusion (2 h), mice were
398 kept in a warm cage in which the temperature was maintained at 35 °C.

399 **Laser speckle contrast imaging (LSCI)**

400 LSCI provides a measure of blood flow velocity by quantifying the extent of blurring of
401 dynamic speckles caused by the motion of red blood cells through the vessels. Briefly,
402 mice were placed under an RFLSI III device (RWD Life Sciences) before and after the
403 suture was successfully inserted through CCA. The skull over both hemispheres was
404 exposed by making an incision along the midline of the scalp. When a 785 nm laser is
405 used to illuminate the brain, it produces a random interference effect that represented
406 blood flow in the form of a speckle pattern. Scattering light was detected by a charge-
407 coupled device (CCD) camera, and the images were acquired by custom software from
408 RWD Life Sciences Company. For each acquisition, a total of 160 images, each of
409 which measured 2048 ×2048 pixels, were collected at 16 Hz.

410 **Tamoxifen**

411 Tamoxifen, 10 mg/ml dissolved in 200 μl corn oil, was administrated intragastrically for 4
412 consecutive days. Prior to further experiments, fluorescent protein expressions in
413 mouse ear vasculatures were first examined. Tamoxifen was administrated at least 2
414 weeks before MCAO surgery.

415 **Immunohistochemistry**

416 Cryosections of fixed mouse brains (50 μm) were handled free-floating and washed for
417 5 minutes in PBS prior to further procedures. Tissue sections were permeablized and
418 blocked in the PBS containing 0.5% Triton and 5% BSA at room temperature for 1 hour.
419 Then, brain sections were incubated with a different primary antibodies, including
420 CD31(1:400, BD, Cat# 557355), VE-Cadherin(1:200, BiCellScientific, Cat# 00105),
421 ERG(1:300, Sigma, Cat# ab110639), GLUT1 (1:300, Sigma, Cat# 07-1401), NeuN
422 (1:300, Merck, Cat# ABN90P), Doublefortin (1:300, Santa clus, Cat# sc-271390), Iba1
423 (1:300, HUABIO, Cat# ET1705-78), GFAP (1:300, Proteintech, Cat# CL488-60190),
424 PDGFR β (1:300, ThermoFisher, Cat# 14-1402-82), NG2 (1:300, Merck, Cat#
425 AB5320) ,CD68 (1:300, BIO-RAD, Cat# MCA1957T), CD45-APC (1:200, Biogend, Cat#
426 103112), Ki67 (1:300, thermoscientific, Cat# RM-9106-S0), F4/80 (1:300, Cell Signaling,
427 Cat# 30325), CD13 (1:300, R&D system, Cat# AF2335), α-SMA-CY3 (1:300, Sigma,
428 Cat# C6198), which were all diluted in the blocking solution (1% percelin, 5% BSA, and
429 0.1% Triton in PBS) at 4 °C overnight. After rinsing in PBS 3 times for 5 minutes each,
430 brain slices were incubated with secondary antibodies accordingly, including donkey
431 anti-mouse IgG (A21202, Thermo Fisher Scientific, 1:1,000) and donkey anti-rabbit IgG

432 (A10040, Thermo Fisher Scientific, 1:1,000). They were diluted in the blocking solution.
433 After a 2-hour incubation, brain slices were washed with PBS three times for 15 minutes
434 each. Finally, Hoechst counterstaining was performed for each specimen. After
435 mounting in an anti-fade mounting medium, images were acquired by using a Zeiss
436 LSM800 laser-scanning confocal microscope with a 20X or 63X objective, with or
437 without Airyscan mode.

438 **Flow cytometry**

439 Primary cell preparation was conducted as described below. Mouse brains were
440 dissected into cold HBSS with glucose and BSA ($HBSS^{++}$, Vendor info) were cut into
441 small pieces by sterile scissors, followed by a centrifuge at 1600 rpm/min for 5 mins to
442 get rid of supernatant. The minced tissues after the centrifuge were incubated with
443 collagenase IV (2.5 mg/ml, ROCHE, Cat# 11088858001) at 37 °C with gentle rotation
444 for 30 min in 2 ml of $HBSS^{++}$. Next, samples were passed through a 70-μm filter and
445 washed with $HBSS^{++}$. To obtain higher cell yield, grind the tissue on the 70-μm filter
446 using a syringe piston and guarantee all tissue pass the filter. The following antibodies
447 in 1:200 dilutions were used: CD31-PE-594 (1:200, Biolegend, Cat# 102520), CD45-
448 APC (1:200, Biogend, Cat# 103112), Ly6C-APC (1:200, Biolegend, Cat# 128016),
449 CD11b-PE (1:200, Biolegend, Cat#101212), Viability dye (1:1000, ThermoFisher,
450 Cat#65-0863-14). Antibody incubation was performed on ice for 30min in HBSS with
451 glucose and BSA. All analyses were performed with CytoFLEX LX-5L1(Beckman).
452 FlowJo x software was used for data analyses.

453 **EdU injection**

454 EdU (200 mg/kg, Alfa Aesar Chemical) was injected intraperitoneally for consecutive 34
455 days since when MCAO was performed. EdU was initially dissolved in DMSO at the
456 stock concentration of XX mg/ml and was diluted with saline prior to injection.

457 **Virus injection**

458 The following adenovirus vector *AAV-CAG-DIO-EGFP* was purchased for ShuMi,
459 Wuhan, China (PT-0168). Half of the one-micron virus was delivered to postnatal day 2
460 mouse pups by intracerebroventricular injection to both sides. After 1.5 months,
461 tamoxifen was administrated. One month later, these mice were subjected to MCAO to
462 induce ischemic stroke.

463 **Radiation and bone marrow transplantation**

464 At two weeks post tamoxifen injection, adult *Cdh5CreERT2:Ai47* mice received
465 radiation (total: 11Gy, 2 times, 5.5Gy per time, interval 2 hours) and bone marrow cell
466 transplantation from wild-type mice with the same genetic background. RBCs were
467 removed from the bone marrow cells by using ACK Lysis Buffer (4 Million cells/mouse).
468 These mice were subjected to MCAO 2 months after bone marrow reconstruction.

469 **Mouse cranial imaging by two-photon microscopy**

470 Adult mice were anesthetized with pentobarbital sodium, and analgesia was provided by
471 subcutaneous injection of 0.2% meloxicam. The scalp was removed, and the skull was
472 exposed and cleaned. A dental drill with a 0.6-mm-diameter bit was used to engrave
473 and thin the bone around the circular craniotomy area at a size of 3 mm. The piece of
474 skull was carefully peeled off with fine-pointed forceps, and a cranial window was
475 generated. A coverslip with a 3-mm diameter was placed on the cranial window, and its

476 perimeter was completely sealed with a 1% agarose gel. The metal headplate was
477 glued onto skull with dental acrylic, through which the mouse brain was fixed on a
478 headplate holder. The headplate holder together with the mouse was placed under a
479 two-photon microscope (FVMPE-RS, Olympus). The cerebral vasculature
480 *Cdh5CreERT2:Ai47* mice was visualized and imaged once a day before and after stroke.
481 All surgeries were performed with sterilized instruments and an environment.

482 **Statistics.**

483 The quantified data in all figures were analyzed with GraphPad Prism 7.0 (La Jolla, CA,
484 USA) and presented as the mean ± SEM with individual data points shown. Unpaired
485 two-tailed Student's t-test was used for assessing the statistical significance between
486 two groups. Statistical significance was determined by calculation of p-value (*$p < 0.05$,
487 **$p < 0.01$, ***$p < 0.001$, and ****$p < 0.0001$, ns: not significant). The repetition of our
488 data is independent biological replicates and the number of replicates for each
489 experiment is noted in the corresponding figure legend.

490 **Data availability**

491 The source data underlying the graphs and charts shown in the figures and tables are
492 provided in Supplementary Data 1. All data generated or analyzed during this study are
493 included in this published article (and its supplementary information file).

494 **Acknowlegements**

495 We thank Xuzhao Li, Zhu Zhu, Dongdong Zhang, Jinze Li, Jiayu Ruan, Lili Zhou for
496 their constructive discussions. We thank Danping Lu for her responsive and timely
497 purchasing support, Jiongfang Xie for sharing AAV virus. We thank the animal facility for

its technical assistance with rodent housing, Biomedical Research center platform for technique support. This work is supported by the National Natural Science Foundation of China (31800864 and 31970969 to J.-M.J, 82101475 to Z.Z.), Westlake startup funds, Westlake Education Foundation and MRIC funds (103536022011) to J.-M.J.; Westlake Education Foundation to B.D.

Author contributions

J.-M.J. conceived the research. T.L. and J.-M.J. designed experiments. T.L. performed all the experiments and data quantification, except for the virus cranial injection. Y.W. performed FACS together with T.L.. Z.Z. conducted some stroke models. Q.G. and B.Z. conducted mouse genotyping.

Competing interests

All authors declare no competing interests.

Fig.1

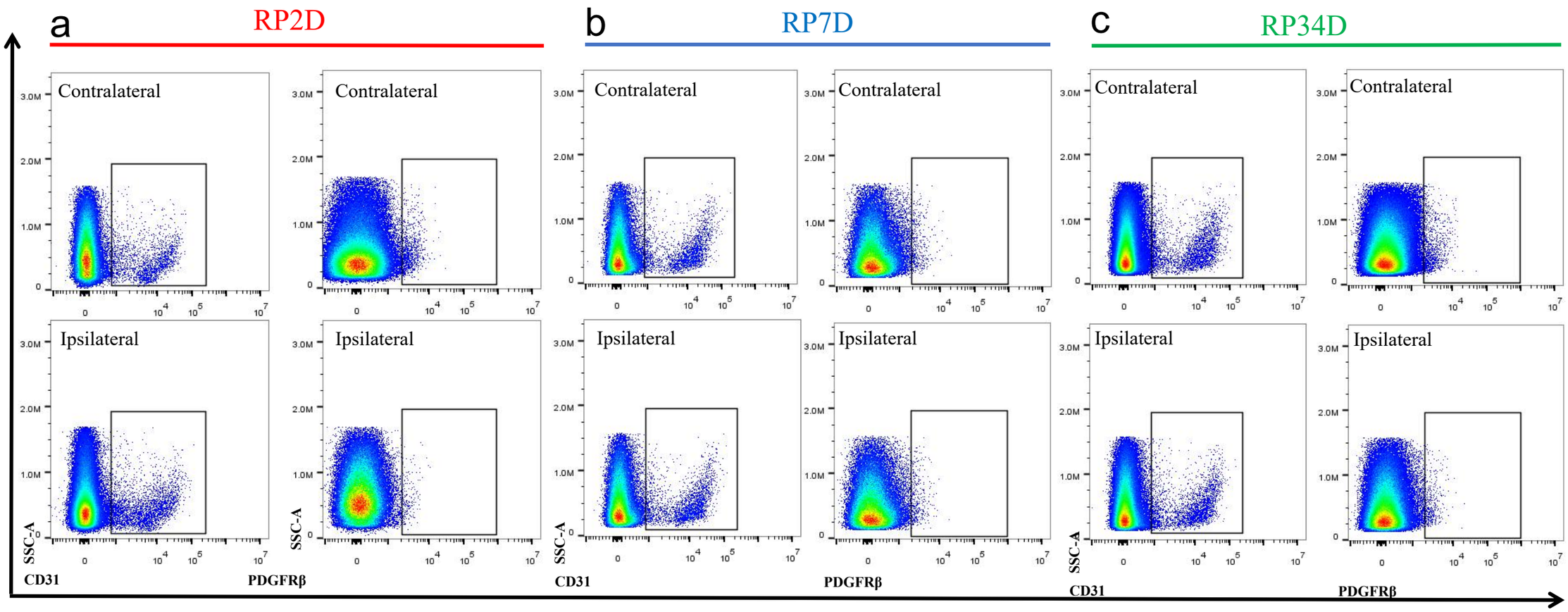
a
RP2D
b
RP7D
c
RP34D
Contralateral
Ipsilateral
SSC-A
CD31
PDGFRβ

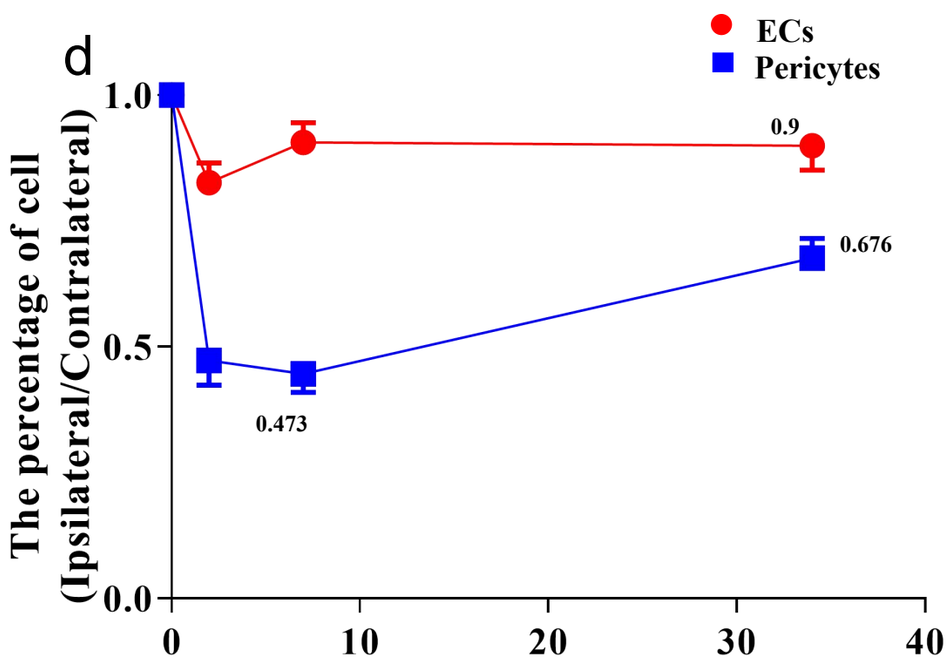
d
ECs
Pericytes
The percentage of cell
(Ipsilateral/Contralateral)
1.0
0.5
0.0
0
10
20
30
40
0.9
0.676
0.473

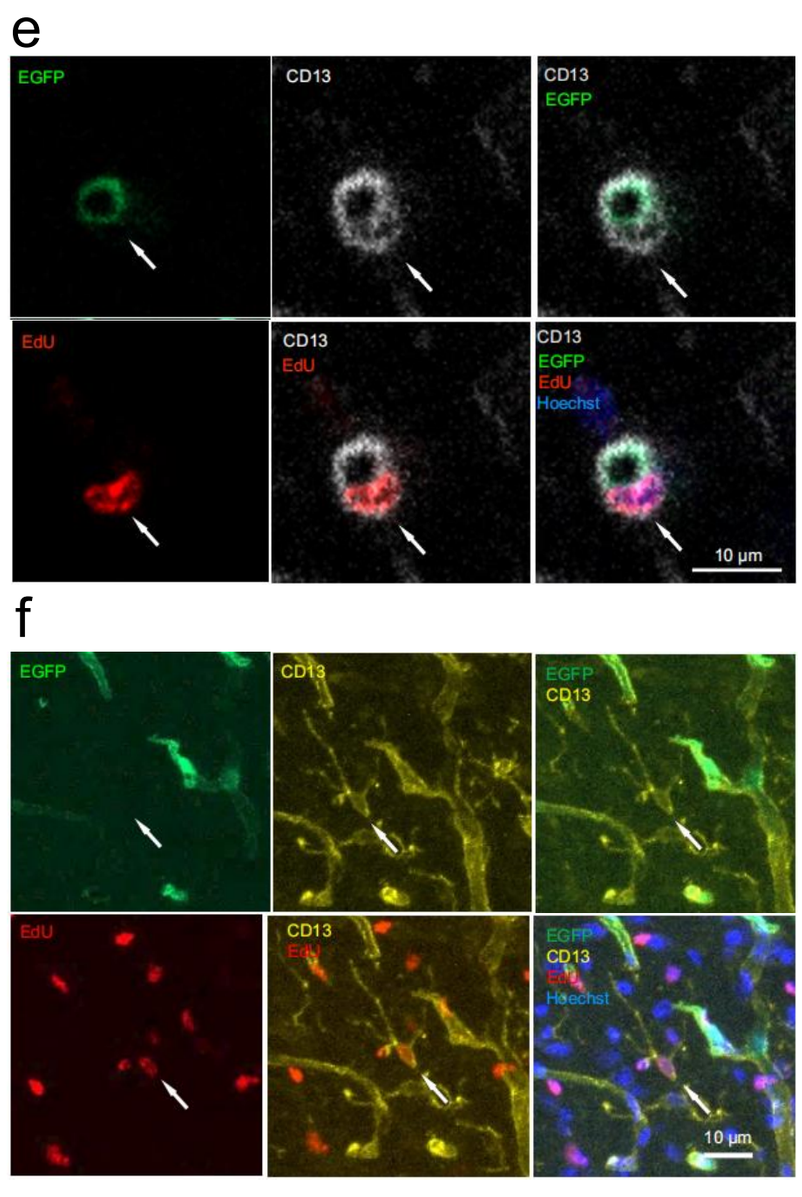
e
EGFP
CD13
EdU
Hoechst
10 μm
f
EGFP
CD13
EdU
Hoechst
10 μm

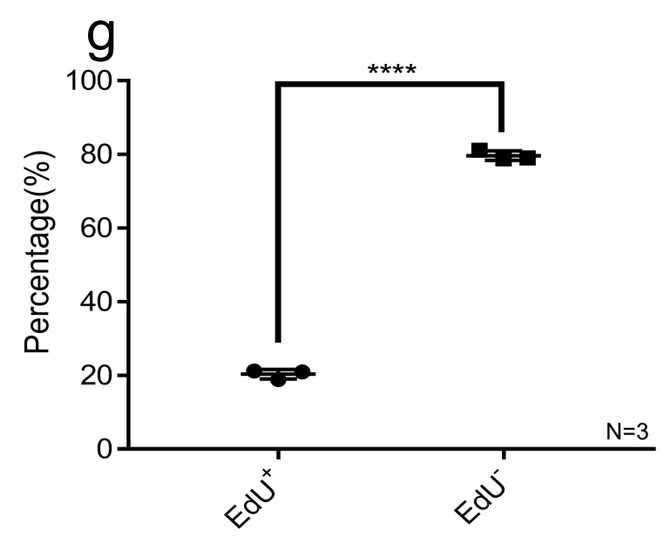
g
Percentage(%)
100
80
60
40
20
0
****
N=3
EdU+
EdU-

519 **Figure legends**

520 **Fig. 1 Ischemic stroke leads to a large number of pericyte death in the acute**
521 **phase, while the number of pericytes gradually increases in the chronic phase of**
522 **ischemia.** a, FACS analysis the number of $CD31^{+}$ECs and $PDGFR\beta^{+}$ pericytes in
523 contralateral control hemisphere (up plot) and ischemic side (down plot) of the same
524 mouse at RP2D. b, FACS analysis the number of $CD31^{+}$ECs and $PDGFR\beta^{+}$ pericytes in
525 contralateral control hemisphere (up plot) and ischemic side (down plot) of the same
526 mouse at RP7D. c, FACS analysis the number of $CD31^{+}$ECs and $PDGFR\beta^{+}$ pericytes in
527 contralateral control hemisphere (up plot) and ischemic side (down plot) of the same
528 mouse at RP34D. d, Quantification of percentages of $CD31^{+}$ECs and $PDGFR\beta^{+}$
529 pericytes at RP2D ,RP7D and RP34D(N=3). e, Illustration of the $EdU^{+\&}CD13^{+}$ pericytes
530 on blood vessel at RP34D. f, Illustration of the $EdU^{+\&}CD13^{+}$ pericytes in brain
531 parenchyma at RP34D. g, Quantification of percentages of $EdU^{+\&}CD13^{+}$ pericytes at
532 R34D(N=3). Data presented as mean ± SEM, ** $P < 0.01$, *** $P < 0.001$, **** $P < 0.0001$.

533

Fig.2

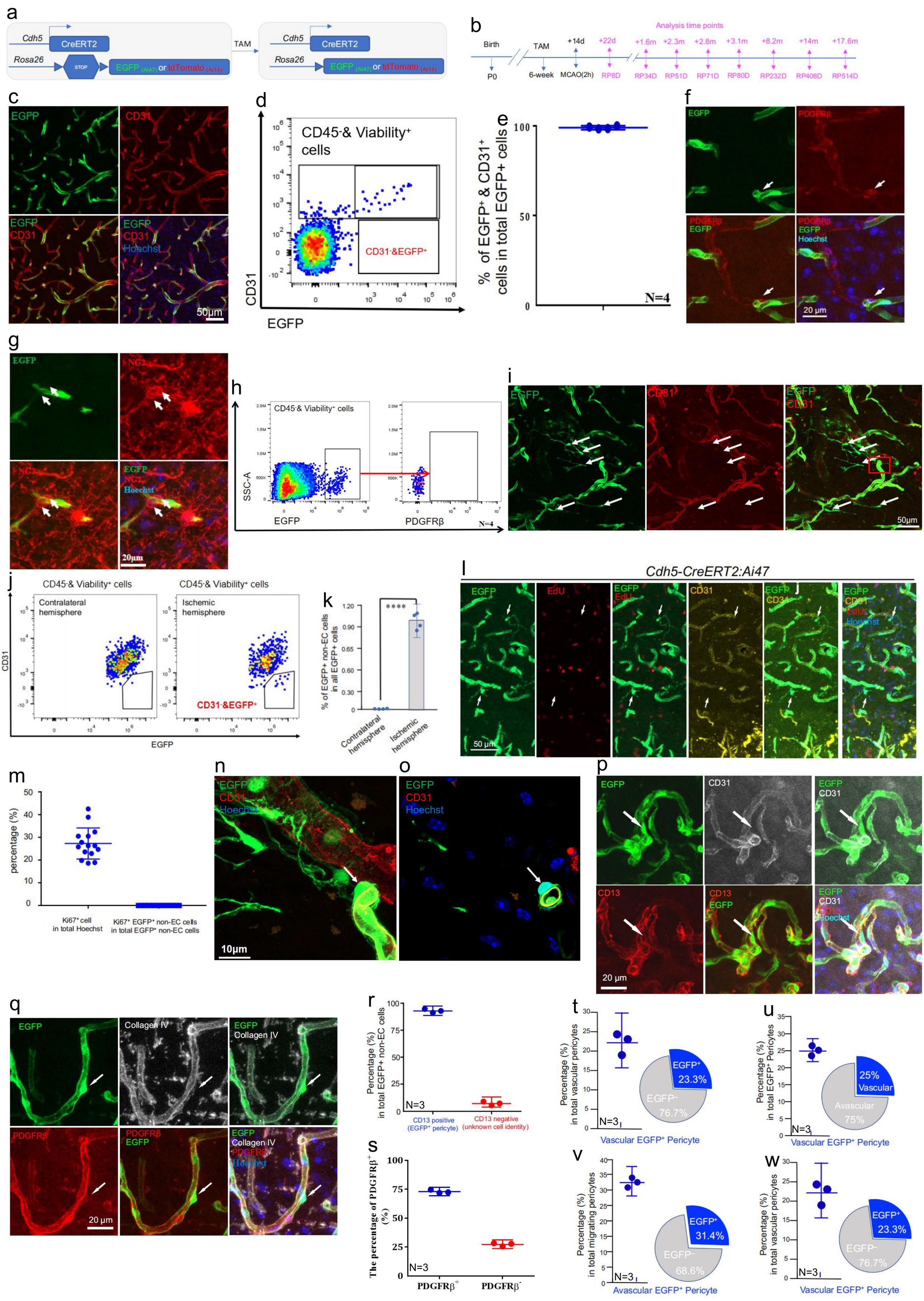
a
Cdh5
CreERT2
Rosa26
STOP
EGFP (Ai47) or tdTomato (Ai14)
TAM
b
Analysis time points
Birth
TAM
+14d
+22d
+1.6m
+2.3m
+2.8m
+3.1m
+8.2m
+14m
+17.6m
P0
6-week
MCAO(2h)
RP8D
RP34D
RP51D
RP71D
RP80D
RP232D
RP408D
RP514D
c
EGFP
CD31
Hoechst
50μm
d
CD45-& Viability+ cells
CD31-&EGFP+
CD31
EGFP
e
% of EGFP+ & CD31+ cells in total EGFP+ cells
N=4
f
PDGFRβ
20 μm
g
NG2
20μm
h
CD45-& Viability+ cells
SSC-A
EGFP
PDGFRβ
N=4
i
50μm
j
CD45-& Viability+ cells
Contralateral hemisphere
Ischemic hemisphere
CD31-&EGFP+
CD31
EGFP
k
% of EGFP+ non-EC cells in all EGFP+ cells
****
Contralateral hemisphere
Ischemic hemisphere
l
Cdh5-CreERT2:Ai47
EdU
CD31
50 μm
m
percentage (%)
Ki67+ cell in total Hoechst
Ki67+ EGFP+ non-EC cells in total EGFP+ non-EC cells
n
10μm
o
p
CD13
20 μm
q
Collagen IV
PDGFRβ
20 μm
r
Percentage (%) in total EGFP+ non-EC cells
N=3
CD13 positive (EGFP+ pericyte)
CD13 negative (unknown cell identity)
s
The percentage of PDGFRβ+ (%)
N=3
PDGFRβ+
PDGFRβ-
t
Percentage (%) in total vascular pericytes
N=3
EGFP+ 23.3%
EGFP- 76.7%
Vascular EGFP+ Pericyte
u
Percentage (%) in total EGFP+ Pericytes
N=3
25% Vascular
Avascular 75%
Vascular EGFP+ Pericyte
v
Percentage (%) in total migrating pericytes
N=3
EGFP+ 31.4%
EGFP- 68.6%
Avascular EGFP+ Pericyte
w
Percentage (%) in total vascular pericytes
N=3
EGFP+ 23.3%
EGFP- 76.7%
Vascular EGFP+ Pericyte

539 **Fig. 2 Genetic tracing of cerebral ECs demonstrates that they can give rise to**
540 **pericyte-like cells via transdifferentiation after ischemic stroke.** a, Illustration of
541 genetic tracing strategy using *Cdh5CreERT2;Ai47* or *Ai14* line. b, Experimental design
542 for tracing periods and reperfusion periods following 2-hour ischemia. c, Confocal
543 images of brain slice vasculatures traced for 1.6 months, stained with EC markers
544 (CD31). d, FACS analysis the specificity of $EGFP^+$ cells using EC marker (CD31). e,
545 Quantification of the specificity of $EGFP^+$ cells using EC marker (CD31)(N=4). f,
546 Confocal images of brain slice $EGFP^+$ cells stained with pericytes markers
547 (PDGFRβand NG2). h, FACS analysis the specificity of $EGFP^+$ cells using pericytes
548 marker (PDGFRβ). i, Confocal images of brain slice $EGFP^+$ cells stained with EC
549 marker (CD31). j, FACS analysis the percentage of $EGFP^+$&$CD31^-$cells using EC
550 marker (CD31). k, Quantification of FACS analysis the percentage of $EGFP^+$&$CD31^-$
551 cells using EC markers (CD31)(N=4). l, Confocal images of brain slice $EGFP^+$ cells
552 stained with proliferation marker (EdU). m, Quantification of confocal images of brain
553 slice $EGFP^+$ cells stained with proliferation markers (EdU).(N=2, 15 brain slices*2). n,
554 Confocal images of brain slice $EGFP^+$ cells stained with ECs marker (CD31). o,
555 Confocal images of brain slice $EGFP^+$ cells stained with ECs marker (CD31)in classic
556 pericyte location. p, Confocal images of brain slice $EGFP^+$ cells stained with pericytes
557 marker (CD13)in classic pericyte location. q, Confocal images of brain slice $EGFP^+$ cells
558 stained with pericytes marker (PDGFRβ)in classic pericyte location. r, Quantification of
559 confocal images of brain slice $EGFP^+$ cells stained with pericytes marker (CD13) in
560 classic pericyte location..(N=3). s, Quantification of confocal images of brain slice
561 $EGFP^+$ cells stained with pericytes marker (PDGFRβ) in classic pericyte location..(N=3).

562 **t**, The transforming efficiency of EGFP$^+$ non-EC cell to pericytes. **u**, Quantification of the
563 percentages of vascular and avascular EGFP$^+$ pericytes. N = 3 mice. **v**, The percentage
564 of avascular EGFP$^+$ pericytes in the total migrating pericyte population after stroke. **w**,
565 The contribution of vascular EGFP$^+$ pericytes to the total vascular pericyte population.
566 Data presented as mean ± SEM, ** $P < 0.01$, *** $P < 0.001$, **** $P < 0.0001$.

567

Fig.3

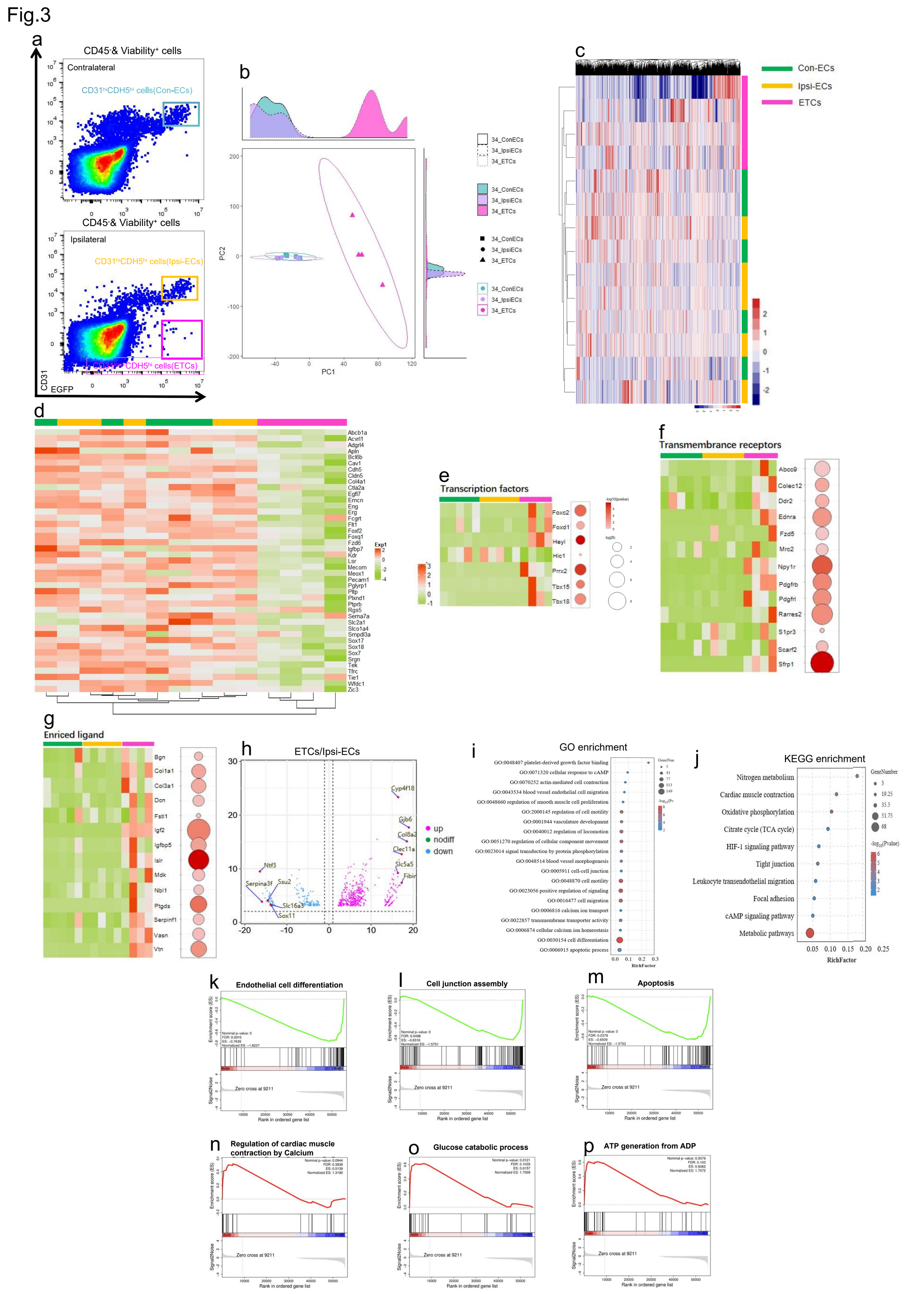
a
CD45-& Viability+ cells
Contralateral
CD31hiCDH5hi cells(Con-ECs)
CD45-& Viability+ cells
Ipsilateral
CD31hiCDH5hi cells(Ipsi-ECs)
CD31loCDH5hi cells(ETCs)
CD31
EGFP
b
PC1
PC2
34_ConECs
34_IpsiECs
34_ETCs
c
Con-ECs
Ipsi-ECs
ETCs
d
e
Transcription factors
Foxc2
Foxd1
Heyl
Hic1
Prrx2
Tbx15
Tbx18
f
Transmembrance receptors
Abcc9
Colec12
Ddr2
Ednra
Fzd5
Mrc2
Npy1r
Pdgfrb
Pdgfrl
Rarres2
S1pr3
Scarf2
Sfrp1
g
Enriced ligand
Bgn
Col1a1
Col3a1
Dcn
Fstl1
Igf2
Igfbp5
Islr
Mdk
Nbl1
Ptgds
Serpinf1
Vasn
Vtn
h
ETCs/Ipsi-ECs
up
nodiff
down
Cyp4f18
Gjb6
Col8a2
Clec11a
Slc5a5
Fibin
Ntf3
Serpina3f
Ssu2
Slc16a3
Sox11
i
GO enrichment
GO:0048407 platelet-derived growth factor binding
GO:0071320 cellular response to cAMP
GO:0070252 actin-mediated cell contraction
GO:0043534 blood vessel endothelial cell migration
GO:0048660 regulation of smooth muscle cell proliferation
GO:2000145 regulation of cell motility
GO:0001944 vasculature development
GO:0040012 regulation of locomotion
GO:0051270 regulation of cellular component movement
GO:0023014 signal transduction by protein phosphorylation
GO:0048514 blood vessel morphogenesis
GO:0005911 cell-cell junction
GO:0048870 cell motility
GO:0023056 positive regulation of signaling
GO:0016477 cell migration
GO:0006816 calcium ion transport
GO:0022857 transmembrane transporter activity
GO:0006874 cellular calcium ion homeostasis
GO:0030154 cell differentiation
GO:0006915 apoptotic process
RichFactor
j
KEGG enrichment
Nitrogen metabolism
Cardiac muscle contraction
Oxidative phosphorylation
Citrate cycle (TCA cycle)
HIF-1 signaling pathway
Tight junction
Leukocyte transendothelial migration
Focal adhesion
cAMP signaling pathway
Metabolic pathways
GeneNumber
RichFactor
k
Endothelial cell differentiation
l
Cell junction assembly
m
Apoptosis
Enrichment score (ES)
Signal2Noise
Zero cross at 9211
Rank in ordered gene list
n
Regulation of cardiac muscle contraction by Calcium
o
Glucose catabolic process
p
ATP generation from ADP

581 **Fig.3 The transcriptome demonstrates that EGFP^{+}&CD31^{-} cells exhibit**
582 **characteristics of pericytes.** a, Illustration the gate of sorting EGFP^{+}&CD31^{-} cells. b.
583 PCA analysis each group similar principal component relationships. c, Heatmap
584 analysis of all genes expression. d, Illustration the expression of endothelial cell
585 markers genes in each group. e, Illustration the expression of pericytes specific
586 transcription factors genes in each group. f, Illustration the expression of pericytes
587 specific membrane proteins genes in each group. g, Illustration the expression of
588 pericytes specific ligand proteins genes in each group. h, Illustration the different genes
589 expression of ETCs group and Ipsi-ECs group. i, Illustration the GO enrichment analysis
590 of ETCs group and Ipsi-ECs group. j, Illustration the KEGG pathway enrichment
591 analysis of ETCs group and Ipsi-ECs group. j-m, Illustration the GSEA analysis
592 analysis of ETCs group and Ipsi-ECs group.
593
594

Fig.4

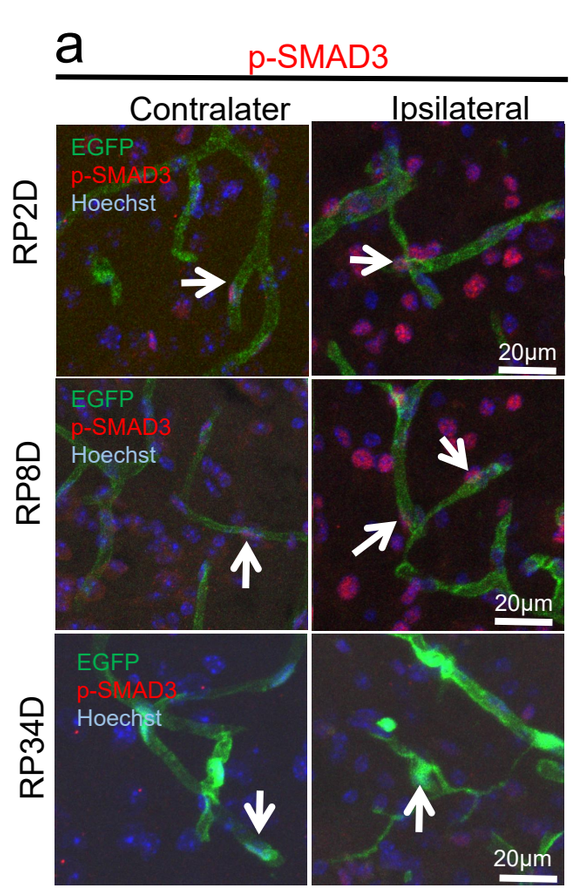
a
p-SMAD3
Contralater
Ipsilateral
RP2D
RP8D
RP34D
EGFP
p-SMAD3
Hoechst
20μm

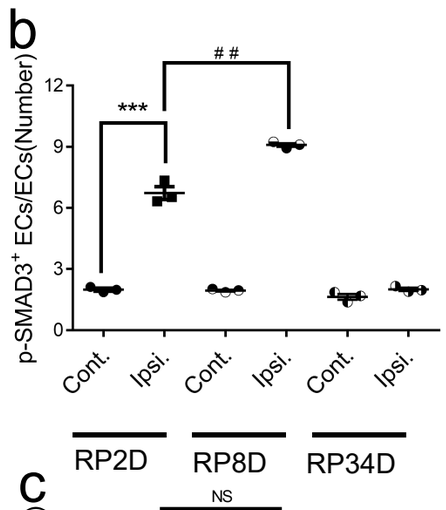
b
p-SMAD3+ ECs/ECs(Number)
***
# #
Cont.
Ipsi.
RP2D
RP8D
RP34D

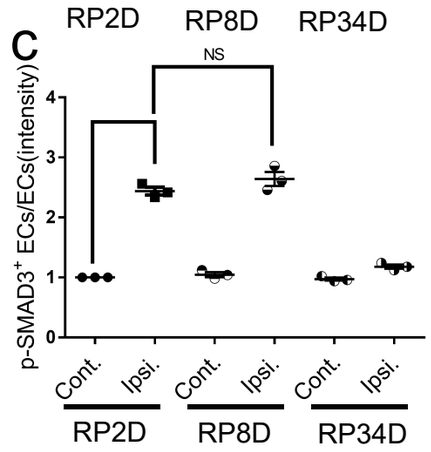
c
p-SMAD3+ ECs/ECs(intensity)
NS
Cont.
Ipsi.
RP2D
RP8D
RP34D

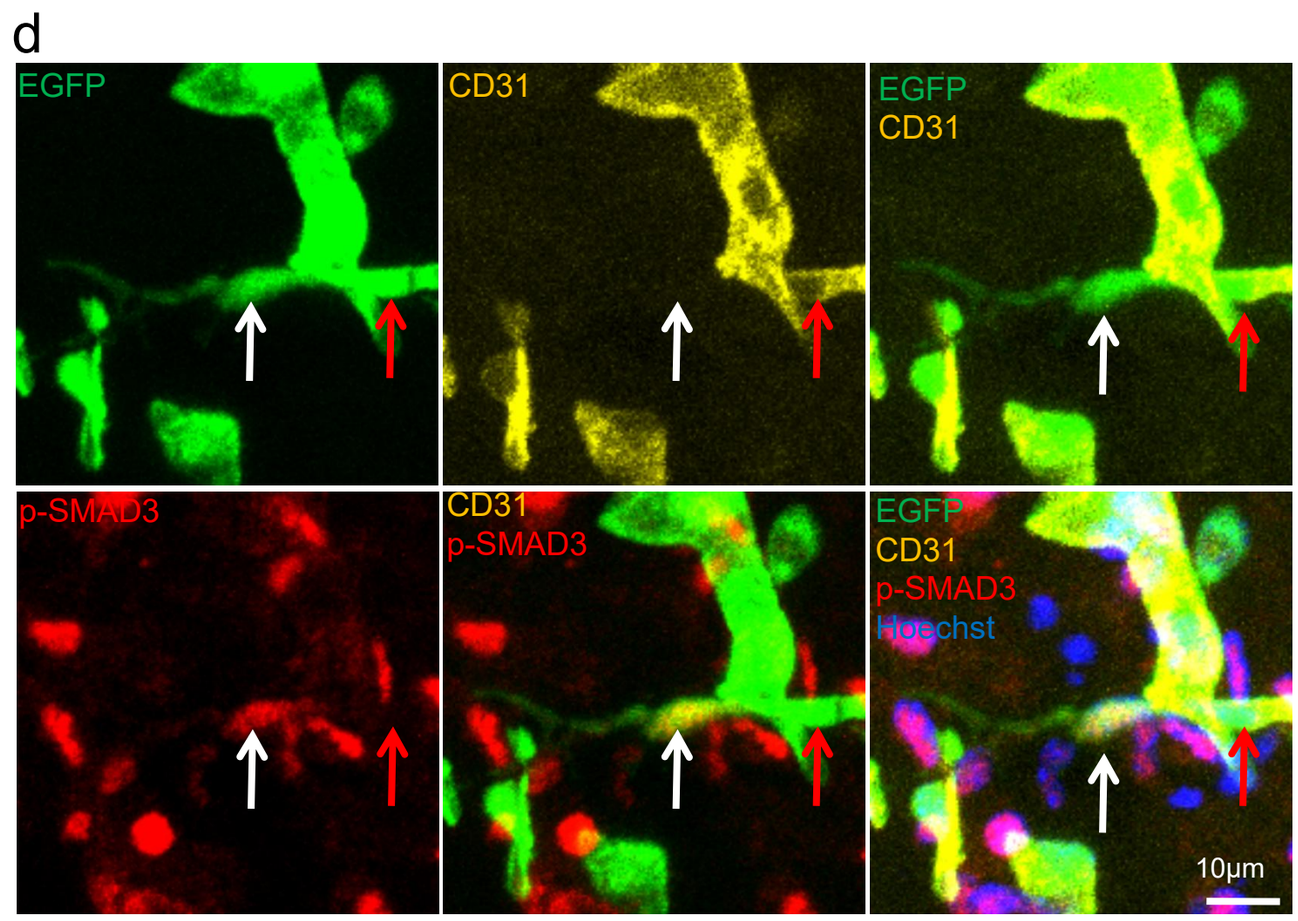
d
EGFP
CD31
p-SMAD3
Hoechst
10μm

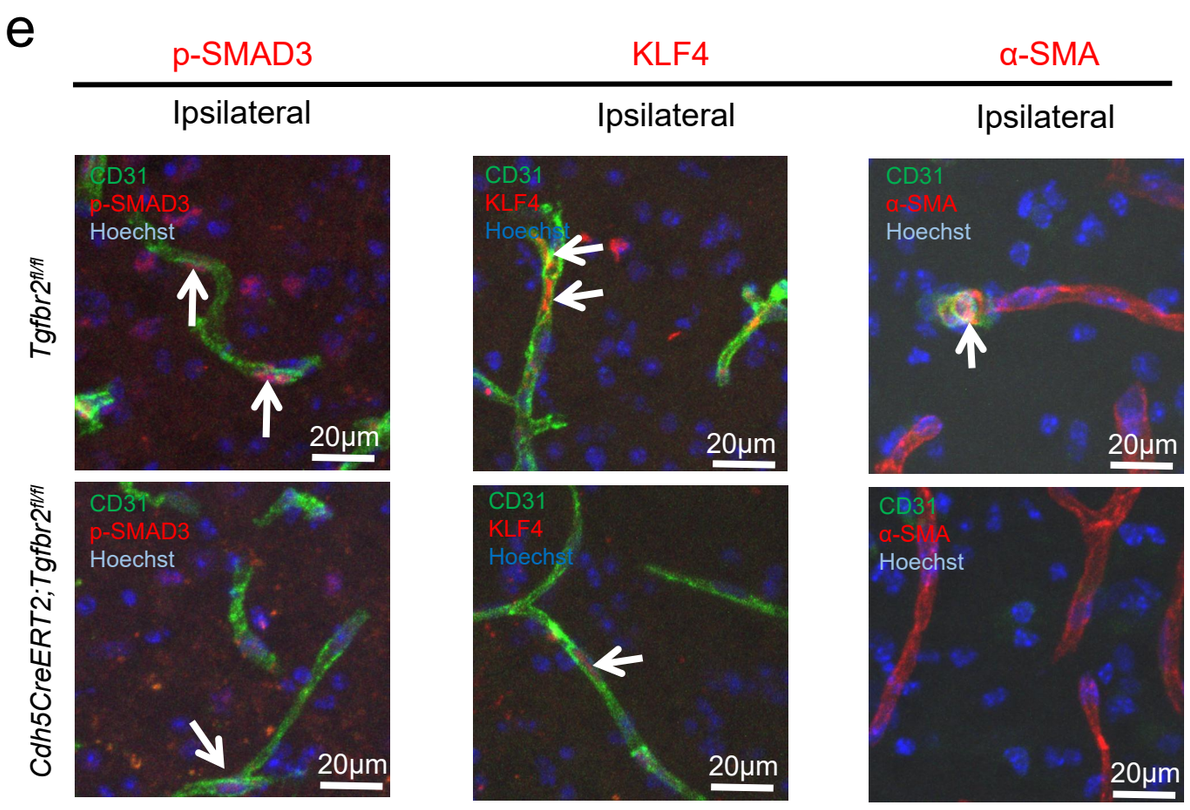
e
p-SMAD3
KLF4
α-SMA
Ipsilateral
Tgfbr2fl/fl
Cdh5CreERT2;Tgfbr2fl/fl
CD31
Hoechst
20μm

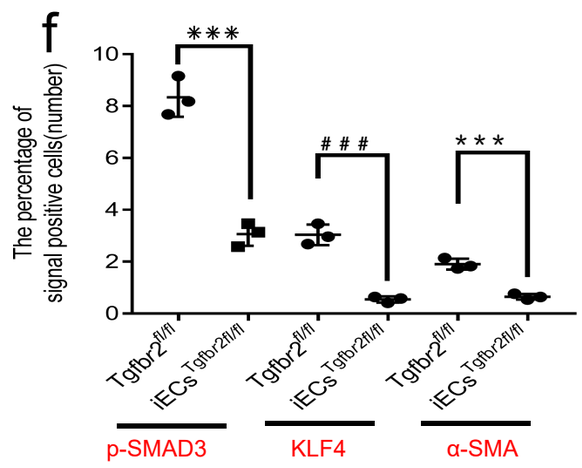
f
The percentage of signal positive cells(number)
***
# # #
* * *
Tgfbr2fl/fl
iECs Tgfbr2fl/fl
p-SMAD3
KLF4
α-SMA

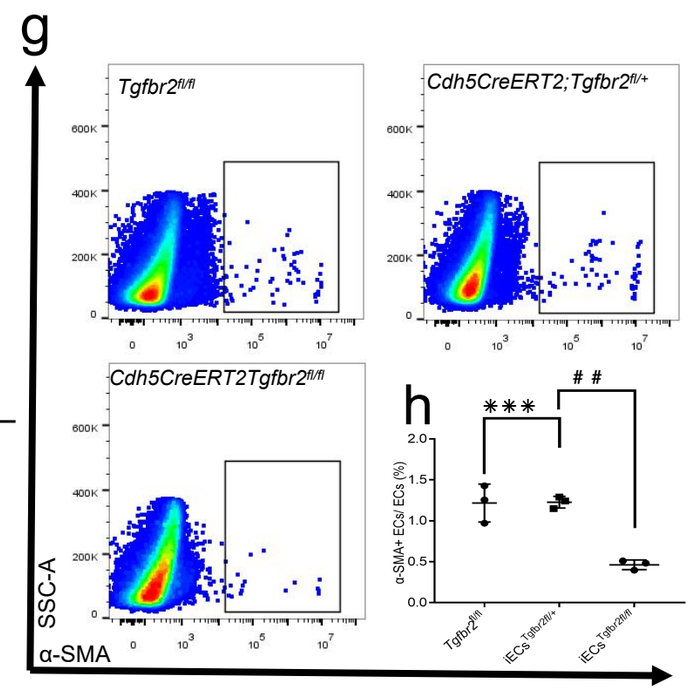
g
Tgfbr2fl/fl
Cdh5CreERT2;Tgfbr2fl/+
Cdh5CreERT2Tgfbr2fl/fl
SSC-A
α-SMA
h
***
# #
α-SMA+ ECs/ ECs (%)

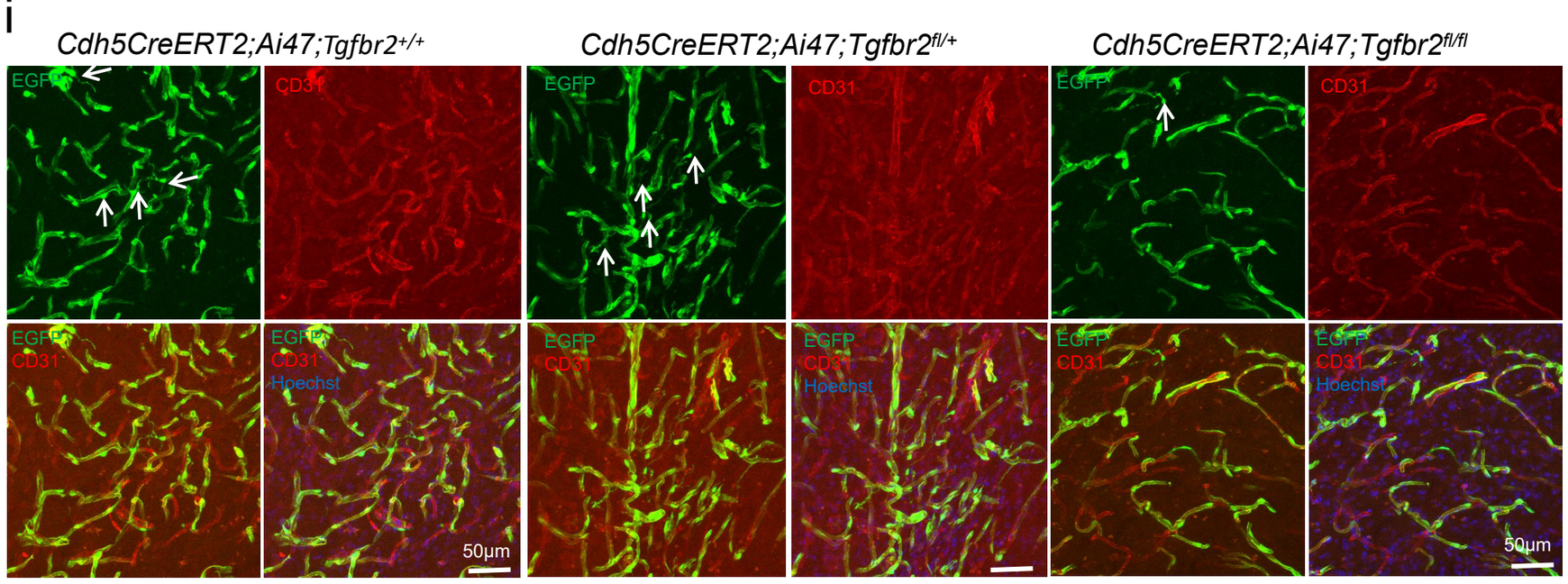
i
Cdh5CreERT2;Ai47;Tgfbr2+/+
Cdh5CreERT2;Ai47;Tgfbr2fl/+
Cdh5CreERT2;Ai47;Tgfbr2fl/fl
EGFP
CD31
Hoechst
50μm

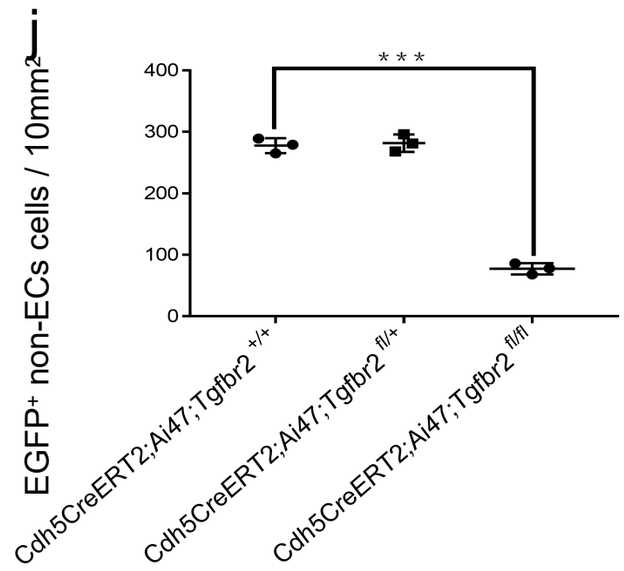
j
EGFP+ non-ECs cells / 10mm2
* * *
Cdh5CreERT2;Ai47;Tgfbr2 +/+
Cdh5CreERT2;Ai47;Tgfbr2 fl/+
Cdh5CreERT2;Ai47;Tgfbr2 fl/fl

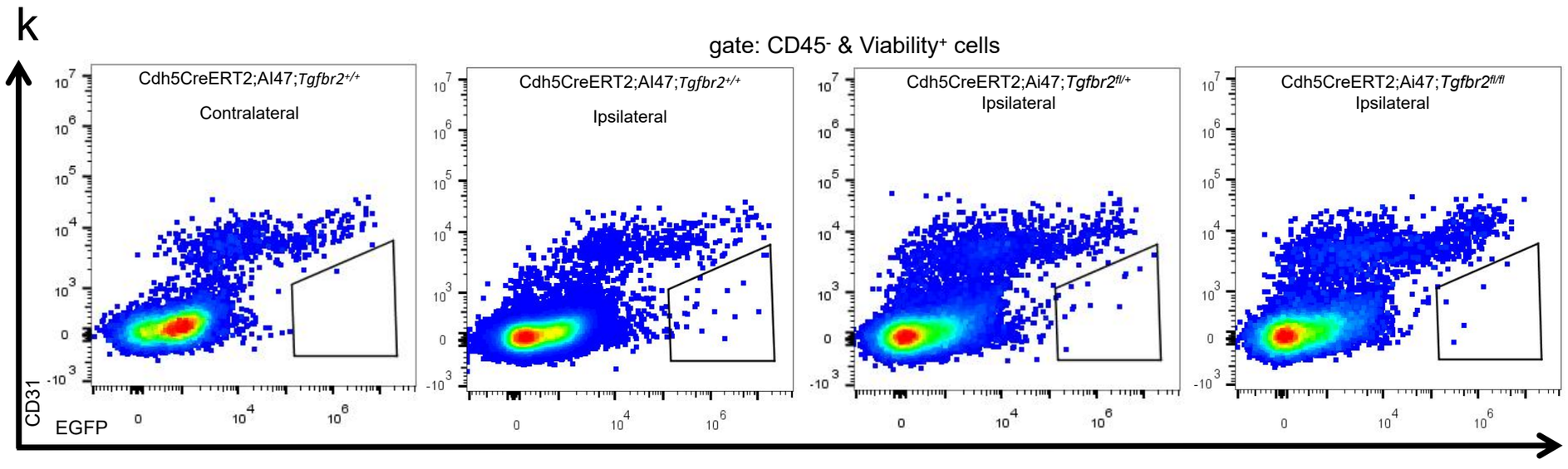
k
gate: CD45- & Viability+ cells
Cdh5CreERT2;Ai47;Tgfbr2+/+
Contralateral
Ipsilateral
Cdh5CreERT2;Ai47;Tgfbr2fl/+
Cdh5CreERT2;Ai47;Tgfbr2fl/fl
CD31
EGFP

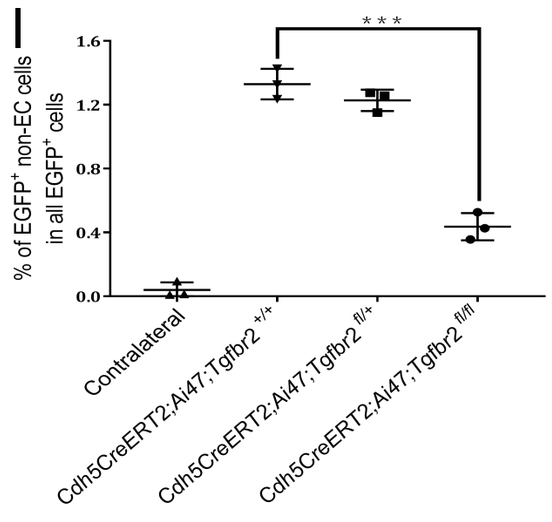
l
% of EGFP+ non-EC cells in all EGFP+ cells
* * *
Contralateral
Cdh5CreERT2;Ai47;Tgfbr2 +/+
Cdh5CreERT2;Ai47;Tgfbr2 fl/+
Cdh5CreERT2;Ai47;Tgfbr2 fl/fl

601 **Fig.4 TGFβ-pSMAD3-EndoMT signaling involved in E-pericytes formation after**
602 **storke.** a, Confocal images of brain slice EGFP$^+$ cells stained with EndoMT marker (p-
603 SMAD3) at RP2D,RP8D and RP34D. b, Quantification the number of confocal images
604 of brain slice EGFP$^+$ cells stained with EndoMT marker (p-SMAD3) at RP2D,RP8D and
605 RP34D.(N=3). c, Quantification the intensity of confocal images of brain slice EGFP$^+$
606 cells stained with EndoMT marker (p-SMAD3) at RP2D,RP8D and RP34D(N=3). d,
607 Confocal images of brain slice EGFP$^+$ cells stained with EndoMT marker (p-SMAD3) at
608 RP8D. e, Confocal images of brain slice EGFP$^+$ cells stained with EndoMT marker (p-
609 SMAD3,KLF4 and α-SMA) at RP2D after specific knockout of Tgfbr2 in endothelial cells.
610 f, Quantification the number of confocal images of brain slice EGFP$^+$ cells stained with
611 EndoMT marker (p-SMAD3,KLF4 and α-SMA) at RP2D after specific knockout of Tgfbr2
612 in endothelial cells. g, FACS analysis the percentage of α-SMA$^+$ ECs using EC marker
613 (CD31) at RP2D after specific knockout of Tgfbr2 in endothelial cells. h,Quantification
614 the FACS analysis the percentage of α-SMA$^+$ ECs using EC marker (CD31)at RP2D
615 after specific knockout of Tgfbr2 in endothelial cells. i, Confocal images of brain slice
616 EGFP$^+$&CD31$^-$ cells stained with ECs marker (CD31) at RP34D after specific knockout
617 of Tgfbr2 in endothelial cells. j, Quantification the confocal images of brain slice
618 EGFP$^+$&CD31$^-$ cells stained with ECs marker (CD31) at RP34D after specific knockout
619 of Tgfbr2 in endothelial cells. k, FACS analysis EGFP$^+$&CD31$^-$ cells stained with ECs
620 marker (CD31) at RP34D after specific knockout of Tgfbr2 in endothelial cells. Data
621 presented as mean ± SEM, ** $P < 0.01$, *** $P < 0.001$, **** $P < 0.0001$.

622

Fig.5

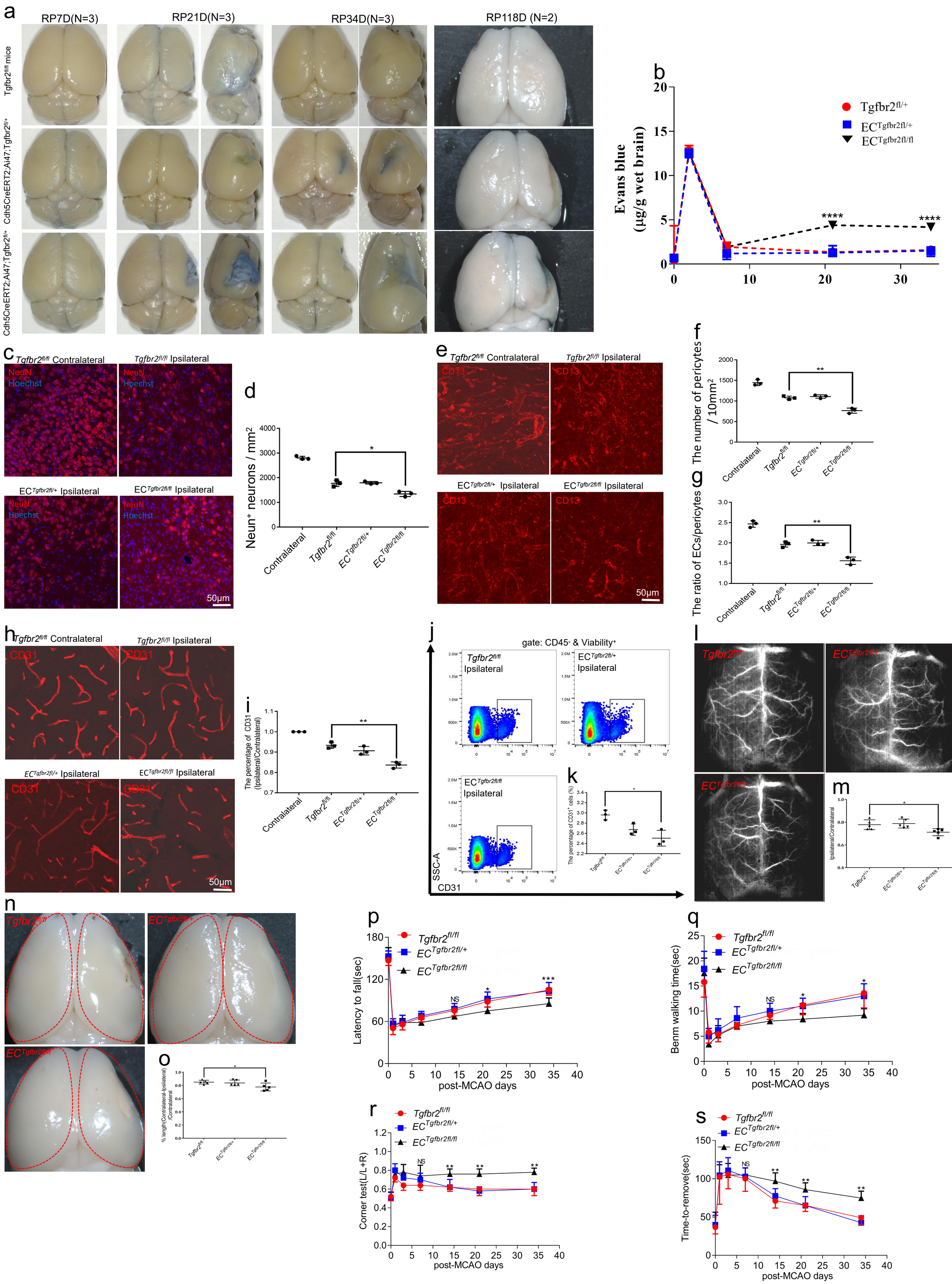
a
RP7D(N=3)
RP21D(N=3)
RP34D(N=3)
RP118D (N=2)
Tgfbr2fl/fl mice
Cdh5CreERT2;Ai47;Tgfbr2fl/+
Cdh5CreERT2;Ai47;Tgfbr2fl/+
b
Evans blue (μg/g wet brain)
Tgfbr2fl/+
ECTgfbr2fl/+
ECTgfbr2fl/fl
c
Tgfbr2fl/fl Contralateral
Tgfbr2fl/fl Ipsilateral
ECTgfbr2fl/+ Ipsilateral
ECTgfbr2fl/fl Ipsilateral
NeuN
Hoechst
50μm
d
Neun+ neurons / mm2
Contralateral
Tgfbr2fl/fl
ECTgfbr2fl/+
ECTgfbr2fl/fl
e
CD13
50μm
f
The number of pericytes / 10mm2
g
The ratio of ECs/pericytes
h
CD31
50μm
i
The percentage of CD31 (Ipsilateral/Contralateral)
j
gate: CD45- & Viability+
SSC-A
CD31
k
The percentage of CD31+ cells (%)
l
m
Ipsilateral/Contralateral
n
o
% length(Contralateral-Ipsilateral) /Contralateral
p
Latency to fall(sec)
post-MCAO days
q
Benm walking time(sec)
r
Corner test(L/L+R)
s
Time-to-remove(sec)

624 **Fig.5 Reducing E-pericytes through specific knockout of Tgfbr2 in endothelial**
625 **cells can impede the recovery of stroke during chronic reperfusion.** a**,** Images of
626 whole brain slice injection with Evans blue after stroke at RP7D, RP21D, RP34D and
627 118D. b, Quantification the whole brain slice injection with Evans blue after stroke at
628 RP2D, RP7D, RP21D and RP34D. c,Confocal images of brain slice neuron stained with
629 marker (Neun) at RP34D. d, Quantification the confocal images of brain slice neuron
630 stained with marker (Neun) at RP34D. e, Confocal images of brain slice pericyte
631 stained with marker (CD13) at RP34D. f, Quantification the confocal images of brain
632 slice pericyte stained with marker (CD13) at RP34D. g, Quantification the confocal
633 images of brain slice the ration of ECs/pericyte (CD13) at RP34D. h, Confocal images of
634 brain slice blood vessel stained with ECs marker (CD31) at RP34D. i, Quantification the
635 confocal images of brain slice blood vessel stained with ECs marker (CD31) at RP34D. j,
636 FACS analysis the percentage of $CD31^+$ ECs at RP34D. k, Quantification the FACS
637 analysis the percentage of $CD31^+$ ECs at RP34D. i, Images of whole brain CBF after
638 stroke at 34D. m, Quantification the images of whole brain CBF after stroke at 34D. n,
639 Images of whole brain volume after stroke at 34D. o, Quantification the images of whole
640 brain volume after stroke at 34D. p, Quantification the time of pole test after stroke at
641 RP0D, RP2D, RP7D, RP14D, RP21D and RP34D. q, Quantification the time of beam
642 walking test after stroke at RP0D, RP2D, RP7D, RP14D, RP21D and RP34D. r,
643 Quantification the time of turning test after stroke at RP0D, RP2D, RP7D, RP14D,
644 RP21D and RP34D. s, Quantification the time of adhesive removal test after stroke at
645 RP0D, RP2D, RP7D, RP14D, RP21D and RP34D. Data presented as mean ± SEM, **
646 $P < 0.01$, *** $P < 0.001$, **** $P < 0.0001$.

Extended Data Fig.1

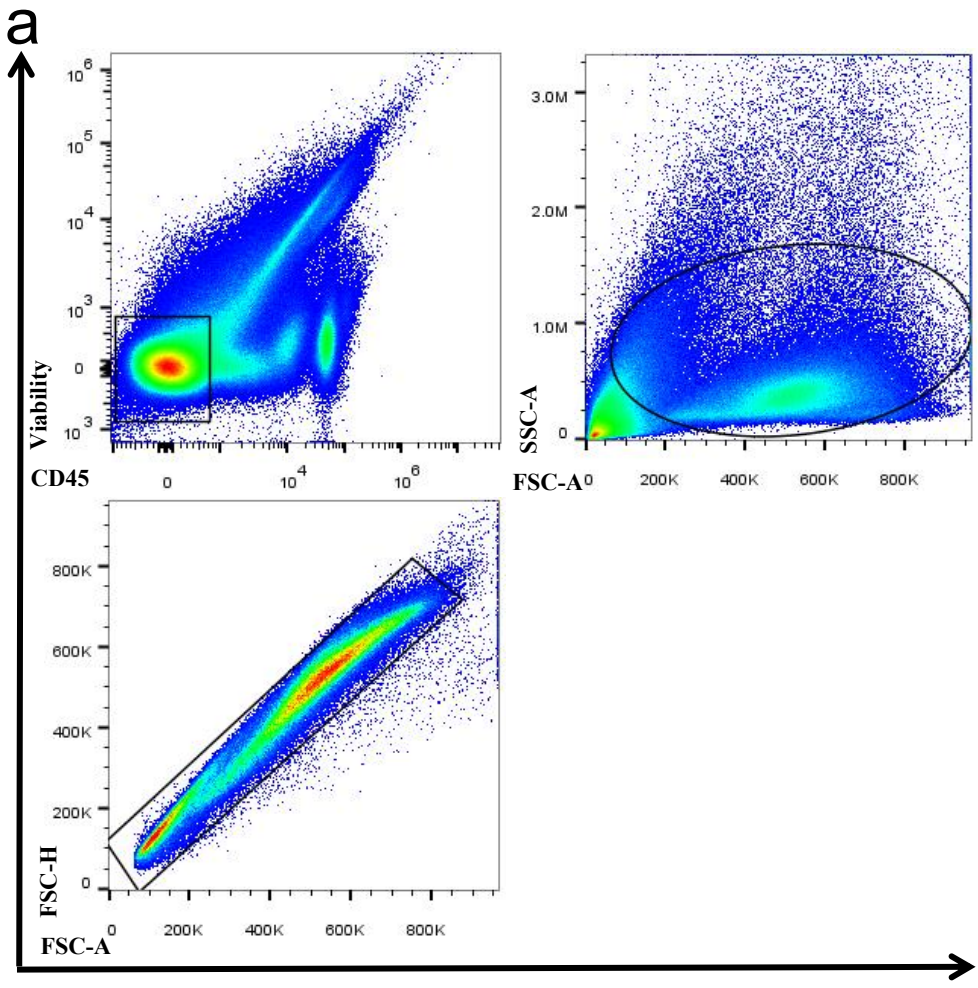

Extended Data Fig. 1 The gate of FACS for the next of experiments. a, The flow of FACS using CD45⁺&Viability⁺ cells for the next analysis and soritng.

Extended Data Fig.2

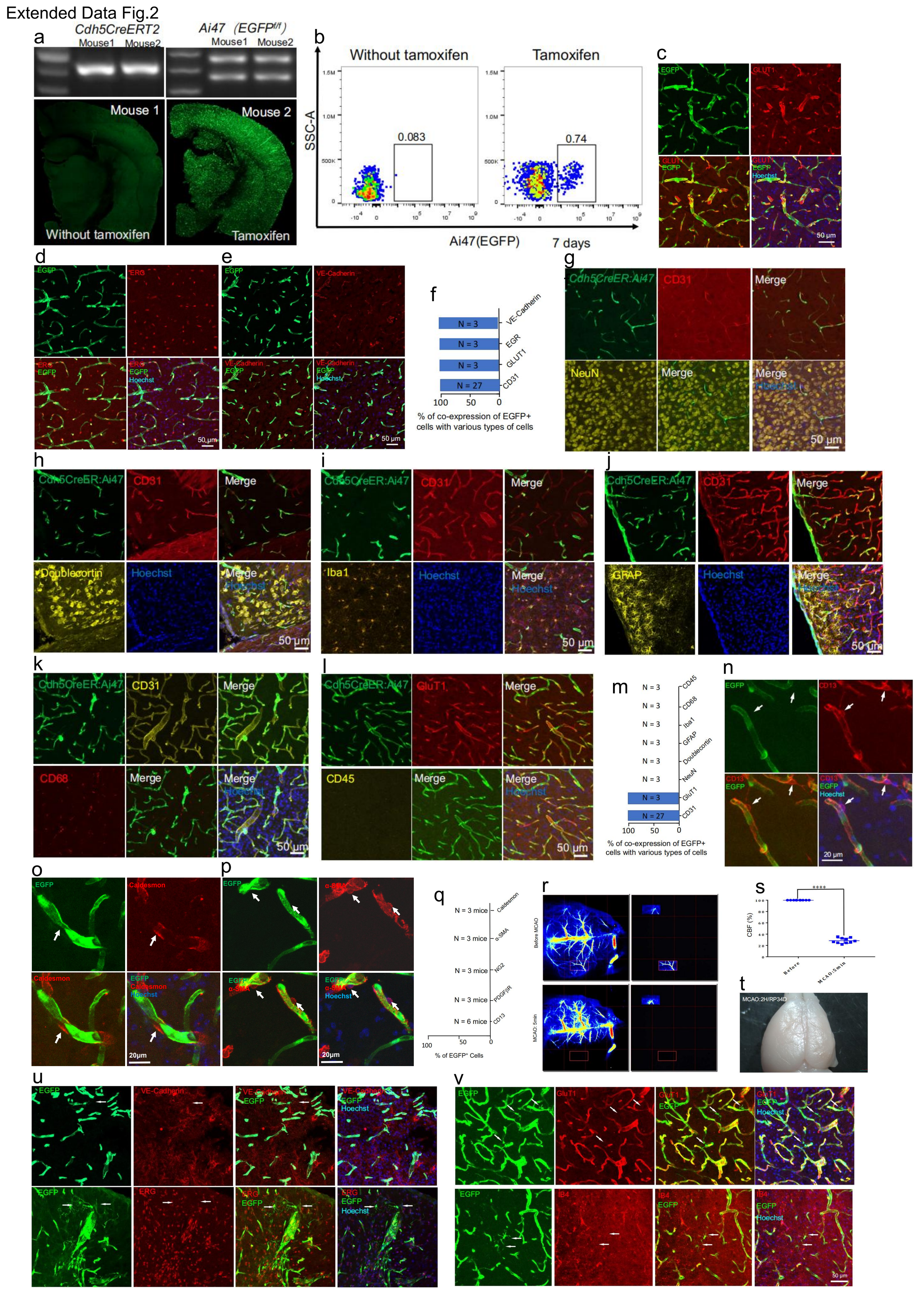

Extended Data Fig.2

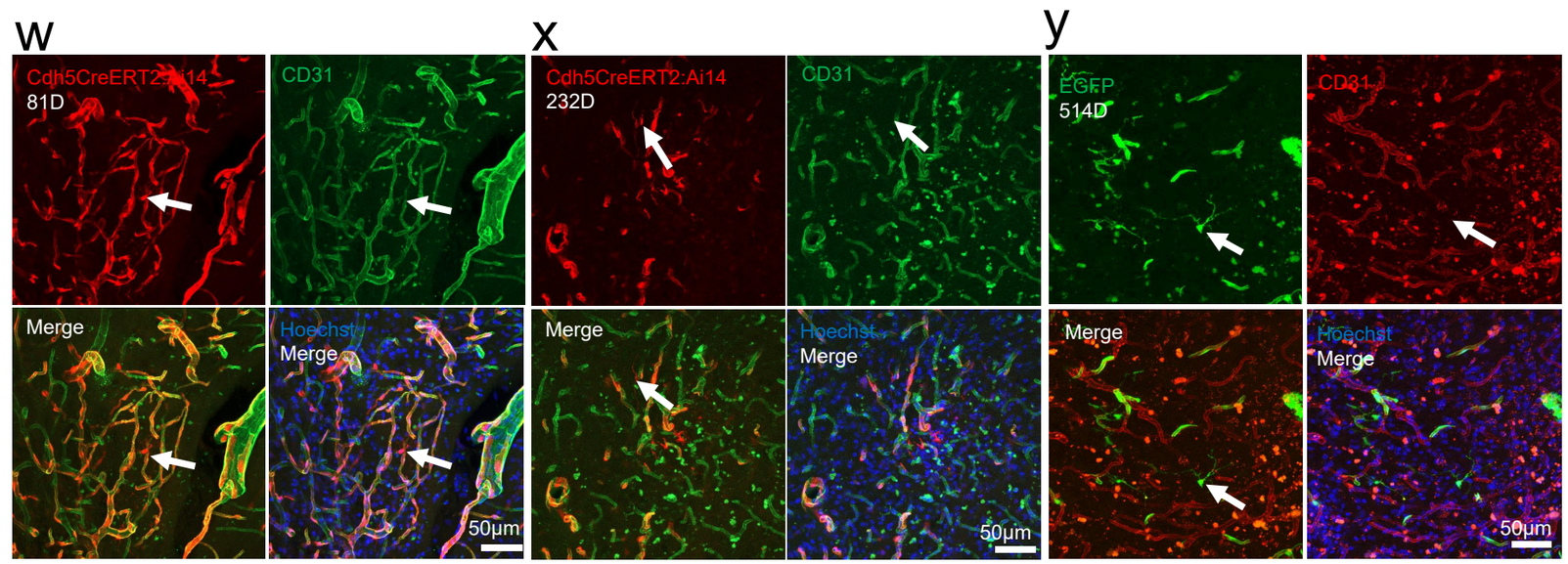

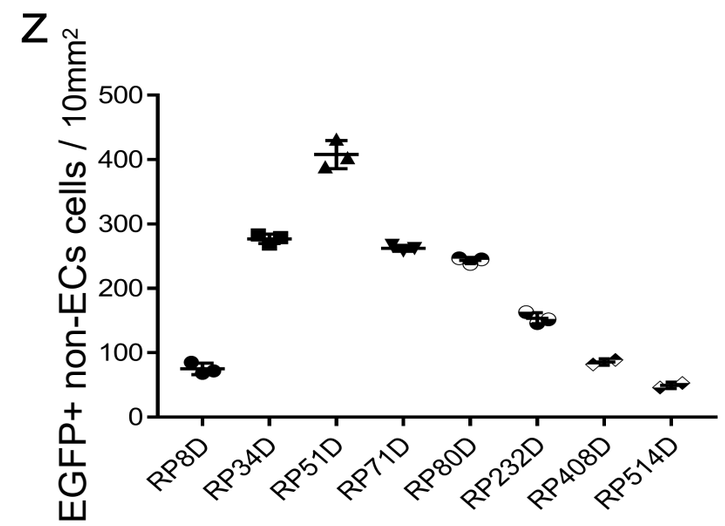

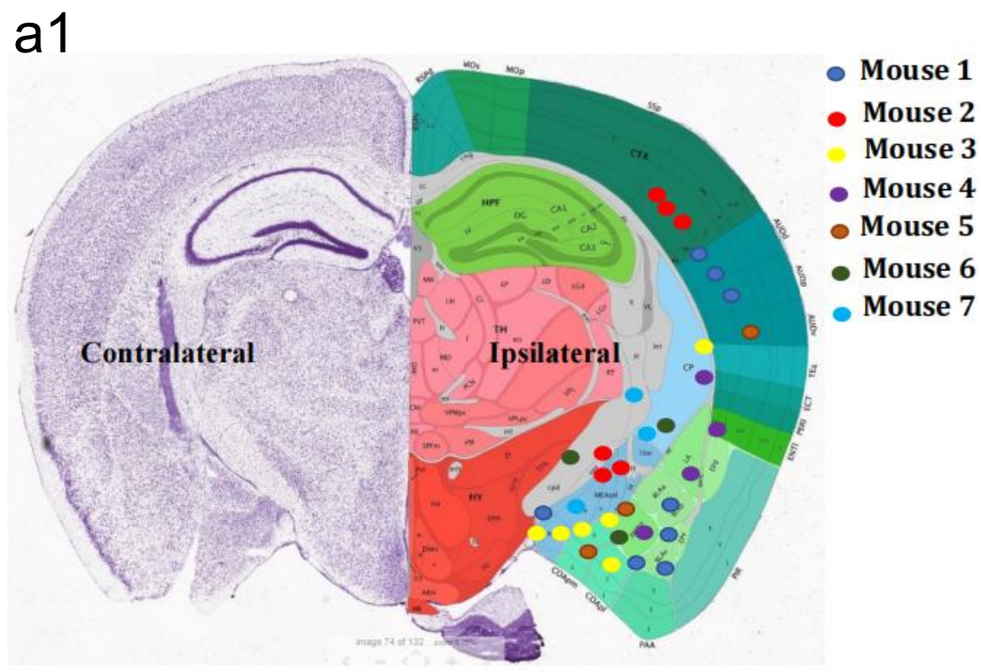

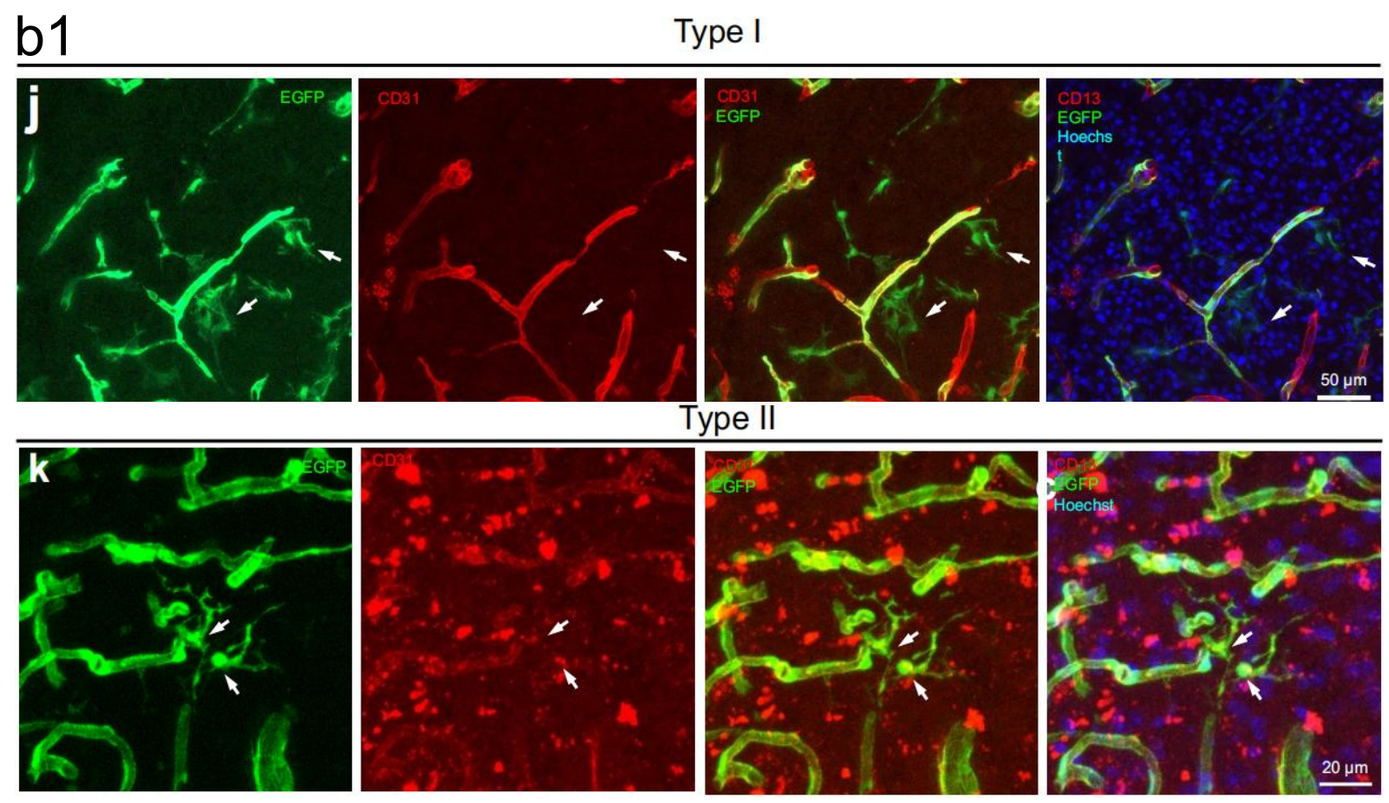

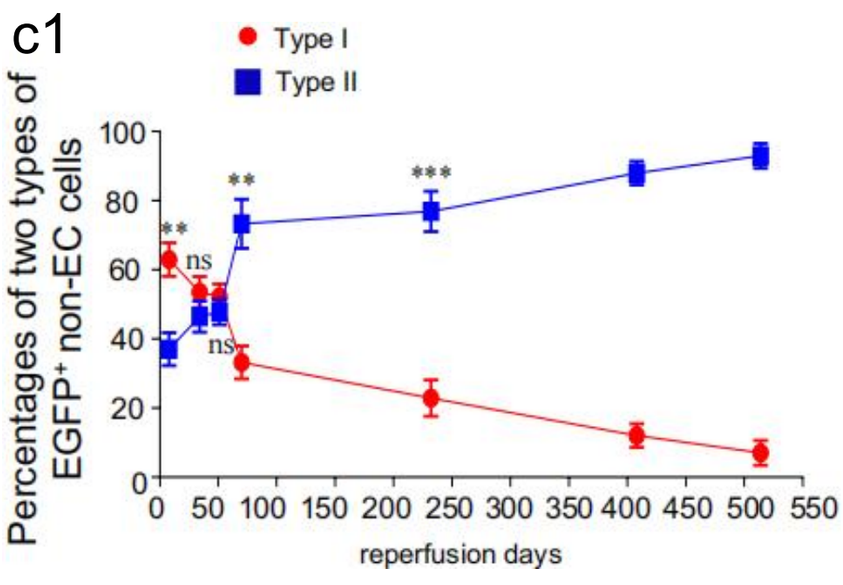

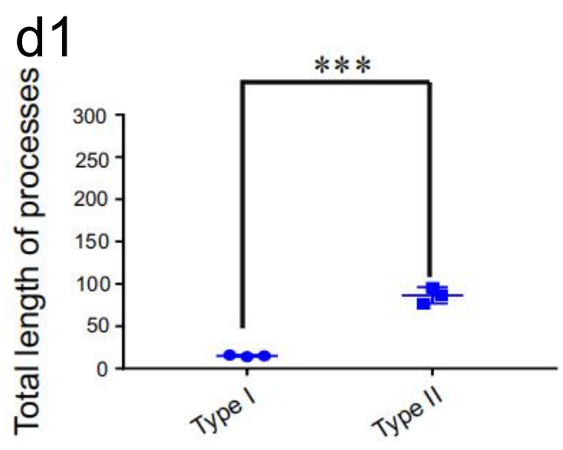

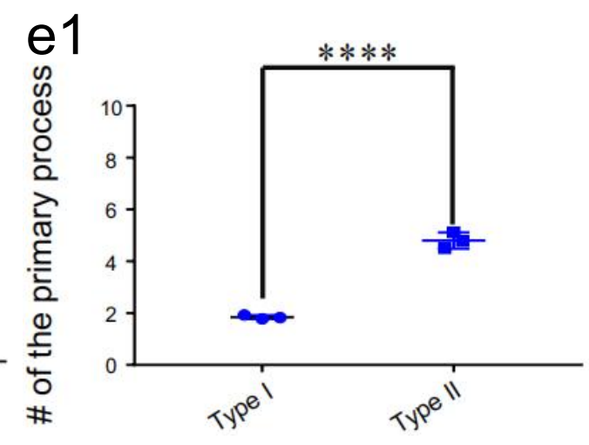

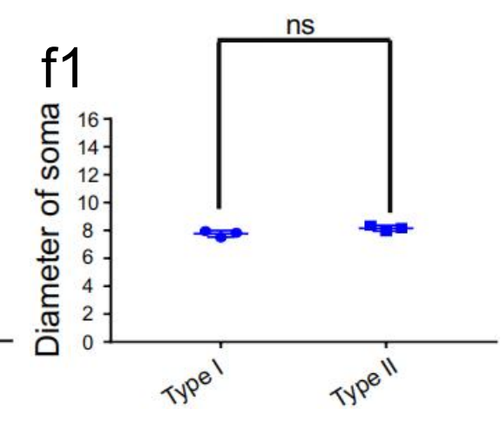

666 **Extended Data Fig. 2 The endothelial cells are capable of undergoing cell fate**
667 **transition after stroke.** a, Confocal images of genetic tracing strategy using
668 *Cdh5CreERT2;Ai47* or *Ai14* line without Tamoxifen. b, FACS analysis genetic tracing
669 strategy using *Cdh5CreERT2;Ai47* or *Ai14* line without Tamoxifen(N=4). c-e, Confocal
670 images of brain slice vasculatures traced for 1.6 months, stained with EC markers
671 (GLUT1, ERG and VE-Cadherin). f, Quantification of confocal images of brain slice
672 EGFP cells stained with EC markers (GLUT1, ERG and VE-Cadherin). g-j, Confocal
673 images of brain slice EGFP cells with other cells markers (NeuN:neuron;
674 Doublecortin:immature neuron; Iba1: microglia; GFAP;astrocyte; CD68:microglia and
675 monocyte-macrophage; CD45:immuce cell). m, Quantification of confocal images of
676 brain slice EGFP cells stained with other cells markers. n-p, Confocal images of brain
677 slice EGFP cells stained with pericytes markers (CD13, Caldesmon and α-SMA). q,
678 Quantification of confocal images of brain slice EGFP cells stained with pericytes
679 markers. r, Images of the CBF of mice after MCAO:2H with LSCI. s, Quantification of
680 the CBF of mice after MCAO:2H with LSCI. t, Images of the whole brain after MCAO:2H.
681 u-v, Confocal images of brain slice $EGFP^+$ cells stained with EC marker (VE-Cadherin ,
682 ERG, GLUT1 and IB4). w-y, Confocal images of brain slice EGFP cells stained with
683 ECs markers (CD31) at RP81D, RP232D and RP514D. z, Quantification of confocal
684 images of brain slice EGFP cells stained with ECs markers (CD31) at RP81D, RP232D
685 and RP514D. a1, Schematic diagram show of the location of $EGFP^+$&$CD31^-$ cells at
686 different RP. b1, Confocal images of brain slice $EGFP^+$&$CD31^-$ cells morphology. c1,
687 Quantification of confocal images of brain slice $EGFP^+$&$CD31^-$ cells morphology. d1-f1,
688 Quantification of confocal images of brain slice $EGFP^+$&$CD31^-$ cells morphology

689 (process length, primary process and diameter of soma). Data presented as mean ±

690 SEM, ** $P < 0.01$, *** $P < 0.001$, **** $P < 0.0001$.

691

Extended Data Fig.3

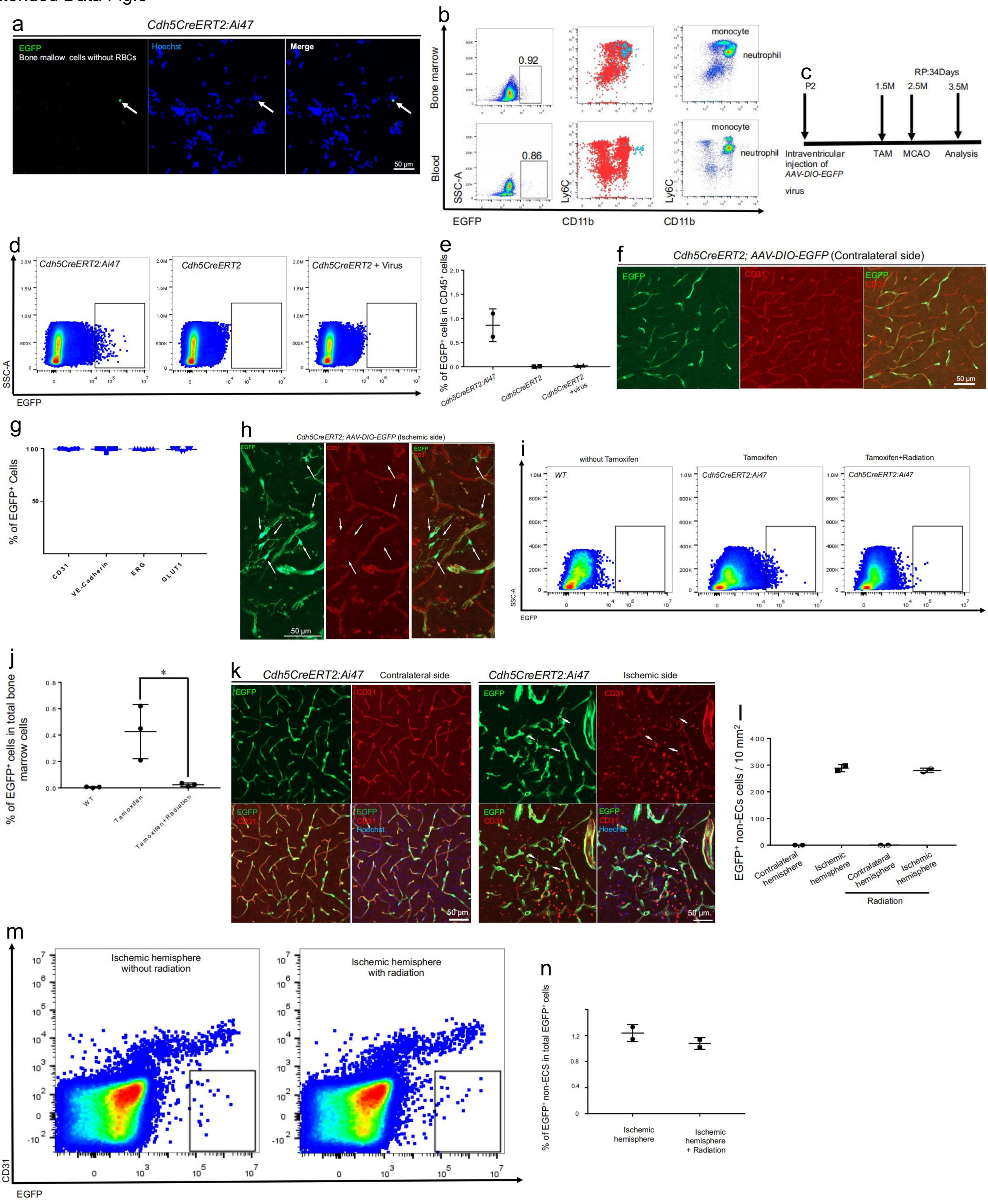

707 **Extended Data Fig. 3 EGFP$^+$&CD31$^-$ cells do not originate from peripheral blood**
708 **non-specific cells labeled in Cdh5CreERT2 mouse.** a, Confocal images of bone
709 marrow cells without RBCs in Cdh5CreERT2 mouse. b, FACS analysis the EGFP+ cells
710 from bone marrow cells without RBCs in Cdh5CreERT2 mouse. c, Illustration of virus
711 strategy using *Cdh5CreERT2* line. d, FACS analysis the EGFP+ cells in bone marrow
712 cells without RBCs form in Cdh5CreERT2 mouse with virus. e, Quantification of FACS
713 analysis the EGFP+ cells in bone marrow cells without RBCs form in Cdh5CreERT2
714 mouse with virus. f, Confocal images of EGFP+ cells in brain from Cdh5CreERT2
715 mouse stained with EC marker CD31. g, Quantification of Confocal images of EGFP+
716 cells in brain from Cdh5CreERT2 mouse stained with EC markers(CD31, VE-Cadherin,
717 ERG and GLUT1). h, Confocal images of EGFP+ cells in brain from Cdh5CreERT2
718 mouse stained with EC marker CD31. i, FACS analysis the percentage of EGFP$^+$ cells
719 after rebuilding bone marrow using radiation. j, Quantification of FACS analysis the
720 percentage of EGFP$^+$ cells after rebuilding bone marrow using radiation. k, Confocal
721 images of EGFP$^+$&CD31$^-$cells in Cdh5CreERT2 with rebuilding bone marrow using
722 radiation. l, Quantification of confocal images of EGFP$^+$&CD31$^-$cells in Cdh5CreERT2
723 with rebuilding bone marrow using radiation. m, FACS analysis EGFP$^+$&CD31$^-$cells in
724 Cdh5CreERT2 with rebuilding bone marrow using radiation. n, Quantification of FACS
725 analysis EGFP$^+$&CD31$^-$cells in Cdh5CreERT2 with rebuilding bone marrow using
726 radiation. Data presented as mean ± SEM, ** $P < 0.01$, *** $P < 0.001$, **** $P < 0.0001$.

727

Extended Data Fig.4

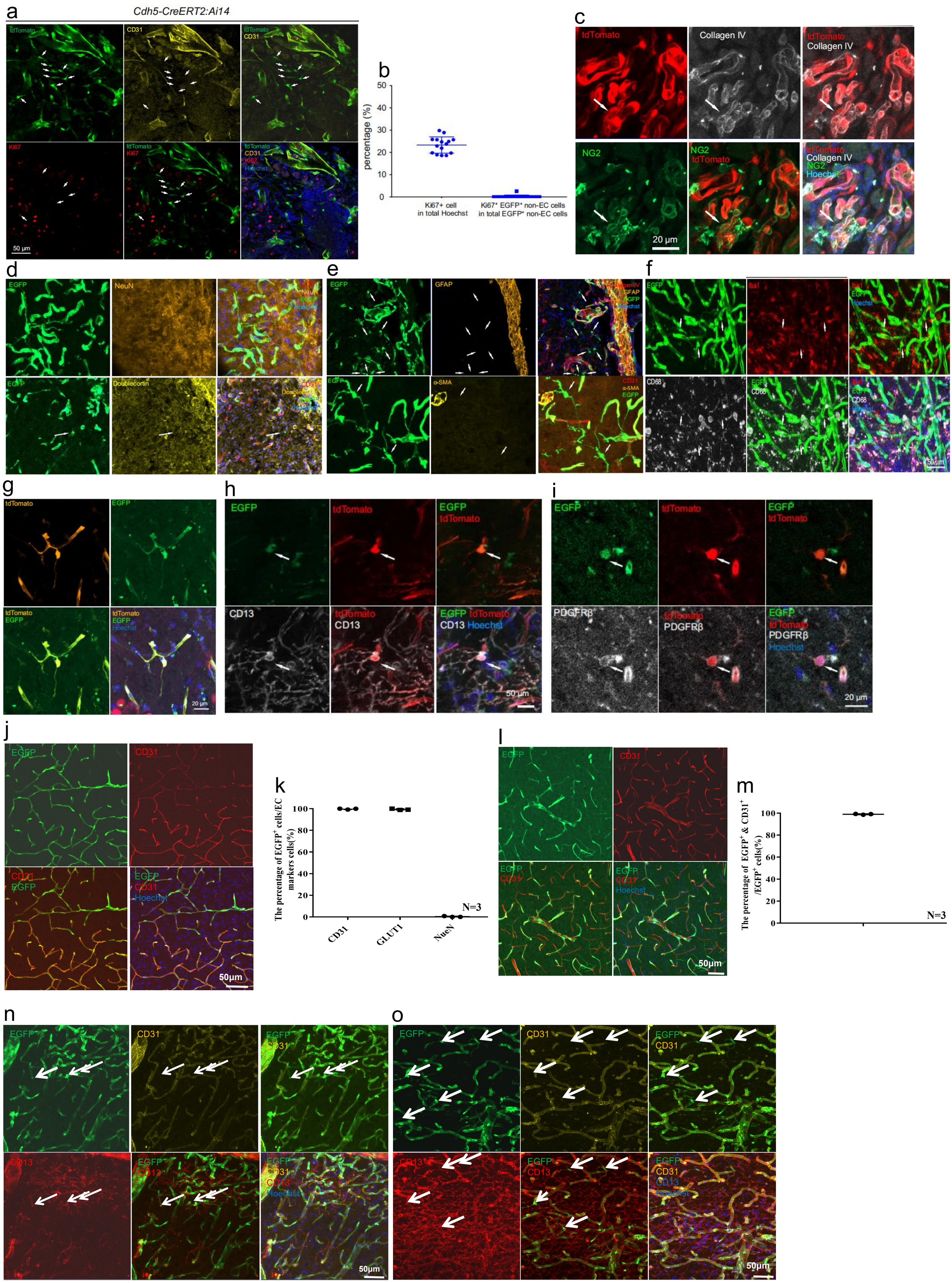

730 **Extended Data Fig. 4 The identification of EGFP$^+$&CD31$^-$ cells is pericyte-like cells.**
731 a, Confocal images of EGFP$^+$&CD31$^-$cells stained with Ki67. b, Quantification of
732 confocal images of EGFP$^+$&CD31$^-$cells stained with Ki67(N=2, 15 brain slice*2). c,
733 Confocal images of EGFP$^+$&CD31$^-$cells stained with pericyte marker(NG2). d-f,
734 Confocal images of EGFP$^+$&CD31$^-$cells stained with other cells markers (NeuN:neuron;
735 Doublecortin:immature neuron; Iba1: microglia; α-SMA:SMC; GFAP;astrocyte; CD68:
736 microglia and monocyte-macrophage). g, Confocal images of EGFP$^+$&CD31$^-$cells in
737 Cdh5CreERT2 mice injection virus. h, Confocal images of EGFP$^+$&CD31$^-$cells stained
738 with pericyte marker(CD13) in Cdh5CreERT2 mice injection virus. i, Confocal images of
739 EGFP$^+$&CD31$^-$cells stained with pericyte marker(PDGFRβ) in Cdh5CreERT2 mice
740 injection virus. j, Confocal images of Tie2Dre;Msfd2a mice brain slice stained with EC
741 marker(CD31). k, Quantification of confocal images of Tie2Dre;Msfd2a mice brain slice
742 stained with EC marker(CD31). l, Confocal images of brain slice from Ai47 mice
743 injection with AAV-Bi30-Cre virus , stained with EC marker(CD31). l, Quantification of
744 confocal images of brain slice from Ai47 mice injection with AAV-Bi30-Cre virus ,
745 stained with EC marker(CD31). n, Confocal images of EGFP$^+$ cells in Tie2Dre;Msfd2a
746 mice brain slice stained with EC marker(CD31) and pericyte marker (CD13). o, Confocal
747 images of EGFP$^+$ cells in Ai47 mice injection with AAV-Bi30-Cre virus brain slice stained
748 with EC marker(CD31) and pericyte marker (CD13). Data presented as mean ± SEM, **
749 $P < 0.01$, *** $P < 0.001$, **** $P < 0.0001$.

750

Extended Data Fig.5

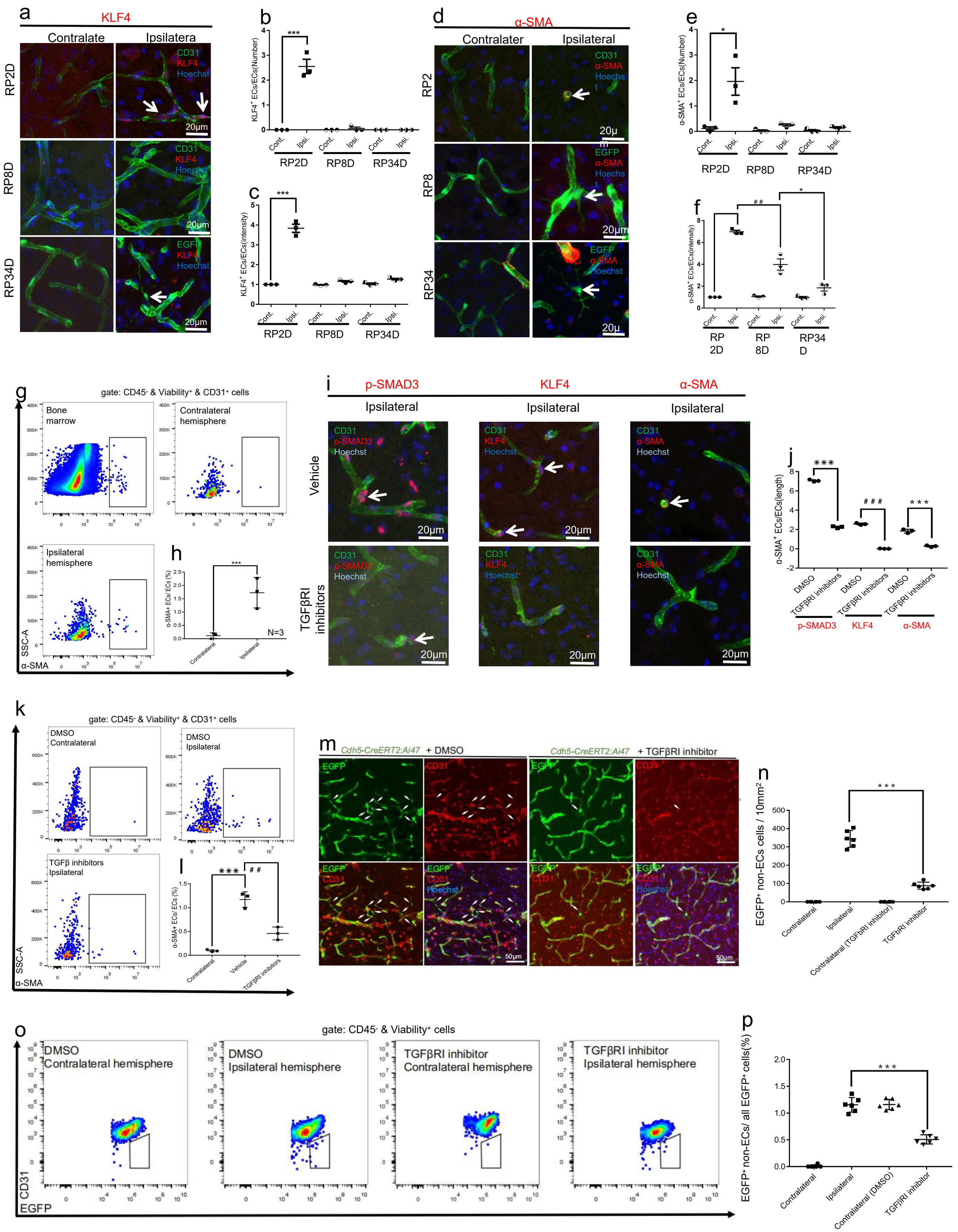

753 **Extended Data Fig. 5 TGFβ-pSMAD3-EndoMT signaling involved in E-pericytes**
754 **formation after storke.** a, Confocal images of brain slice EGFP$^+$ cells stained with
755 EndoMT marker (KLF4) at RP2D,RP8D and RP34D. b, Quantification the number of
756 confocal images of brain slice EGFP$^+$ cells stained with EndoMT marker (KLF4) at
757 RP2D,RP8D and RP34D.(N=3). c, Quantification the intensity of confocal images of
758 brain slice EGFP$^+$ cells stained with EndoMT marker (KLF4) at RP2D,RP8D and
759 RP34D(N=3). d, Confocal images of brain slice EGFP$^+$ cells stained with EndoMT
760 marker (α-SMA) at RP2D,RP8D and RP34D. e, Quantification the number of confocal
761 images of brain slice EGFP$^+$ cells stained with EndoMT marker (α-SMA) at at
762 RP2D,RP8D and RP34D. f, Quantification the indensity of confocal images of brain slice
763 EGFP$^+$ cells stained with EndoMT marker (α-SMA) at at RP2D,RP8D and RP34D. g,
764 FACS analysis the percentage of α-SMA$^+$ ECs using EC marker (CD31) at RP2D.
765 h,Quantification the FACS analysis the percentage of α-SMA$^+$ ECs using EC marker
766 (CD31)at RP2D. i, Confocal images of brain slice EGFP$^+$cells stained with EndoMT
767 markers (p-SMAD3, KLF4 and α-SMA) at RP2D after using TGFBR2 inhibitors. j,
768 Quantification the confocal images of brain slice EGFP$^+$cells stained with EndoMT
769 markers (p-SMAD3, KLF4 and α-SMA) at RP2D after using TGFBR2 inhibitors. k, FACS
770 analysis the percentage of α-SMA$^+$ ECs using EC marker (CD31) at RP2D after using
771 TGFBR2 inhibitors. l, Quantification the FACS analysis the percentage of α-SMA$^+$ ECs
772 using EC marker (CD31) at RP2D after using TGFBR2 inhibitors. m, Confocal images of
773 brain slice EGFP$^+$ cells stained with EC marker (CD31) at RP34D after using TGFBR2
774 inhibitors. n, Quantification the confocal images of brain slice EGFP$^+$ cells stained with
775 EC marker (CD31) at RP34D after using TGFBR2 inhibitors. o, FACS analysis brain

776 slice EGFP^{+} cells stained with EC marker (CD31) at RP34D after using TGFBR2
777 inhibitors. p, Quantification the FACS analysis brain slice EGFP^{+} cells stained with EC
778 marker (CD31) at RP34D after using TGFBR2 inhibitors. Data presented as mean ±
779 SEM, ** $P < 0.01$, *** $P < 0.001$, **** $P < 0.0001$.

780

Extended Data Fig.6

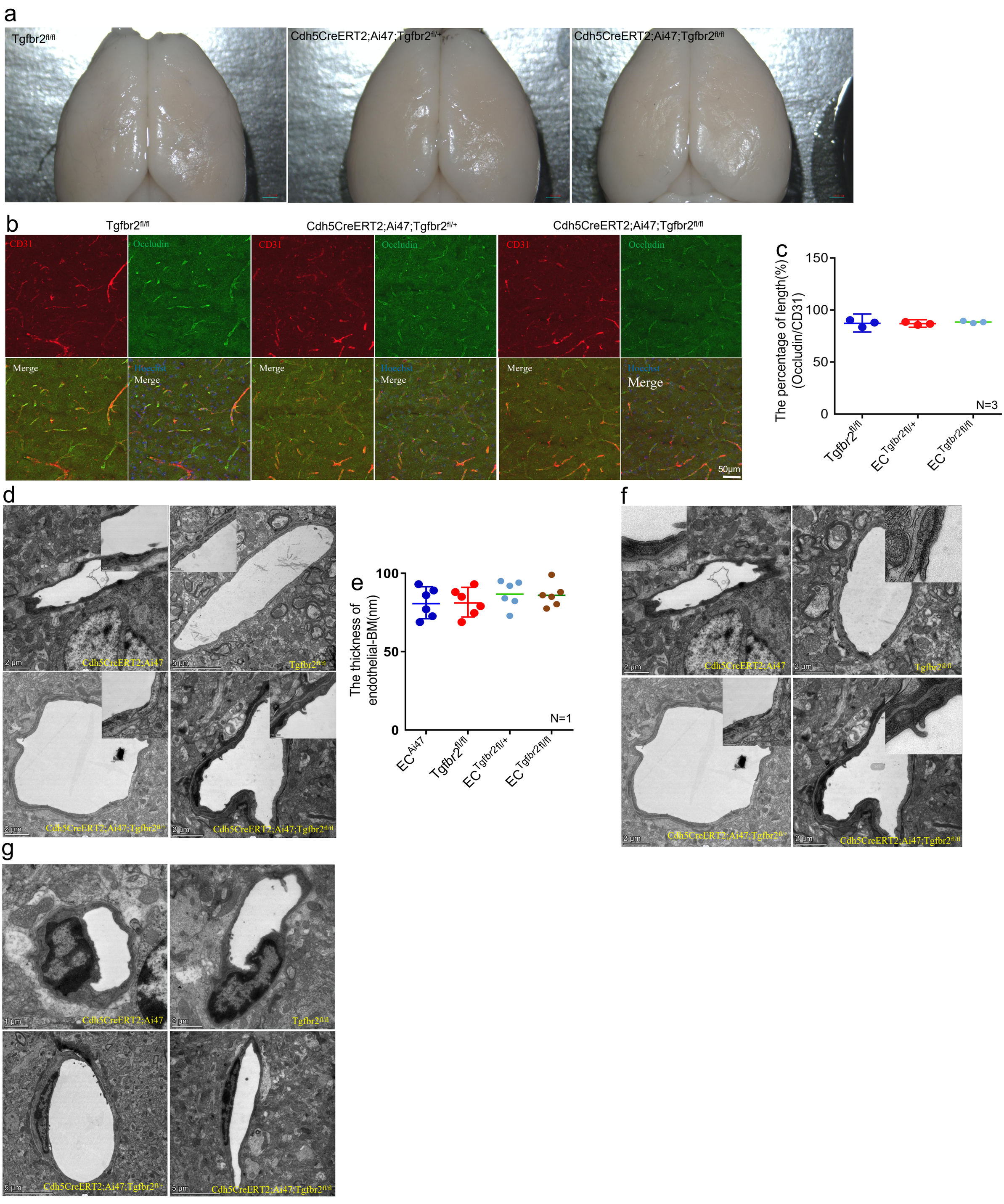

795 **Extended Data Fig. 6 Knocking out Tgfbr2 ECs from adult mouse does not affect**
796 **the BBB function.** a, Images of the whole brain injection with Evans blue in normal
797 state. b, confocal images of brain slice $CD31^+$ ECs stained with BBB marker (ZO-1) in
798 normal state. c, Quantification of confocal images of brain slice $CD31^+$ ECs stained
799 with BBB marker (ZO-1) in normal state. d, Images of the thickness of basement
800 membrane brain slice useing EM in normal state. e, Quantification of images of the
801 thickness of basement membrane in brain slice using EM in normal state. f, Images of
802 the endothelial tight junction in brain slice using EM in normal state. g, Images of the
803 endothelial transcytosis in brain slice using EM in normal state. Data presented as
804 mean ± SEM, ** $P < 0.01$, *** $P < 0.001$, **** $P < 0.0001$.

805

815 1. Kuriakose, D. & Xiao, Z. Pathophysiology and Treatment of Stroke: Present
816 Status and Future Perspectives. *Int J Mol Sci* **21** (2020).
817 2. Martino, G. How the brain repairs itself: new therapeutic strategies in
818 inflammatory and degenerative CNS disorders. *Lancet Neurol* **3**, 372-378 (2004).
819 3. Zhao, L.R. & Willing, A. Enhancing endogenous capacity to repair a stroke-
820 damaged brain: An evolving field for stroke research. *Prog Neurobiol* **163-164**, 5-
821 26 (2018).
822 4. Hall, C.N. *et al.* Capillary pericytes regulate cerebral blood flow in health and
823 disease. *Nature* **508**, 55-60 (2014).
824 5. Díaz-Flores, L., Gutiérrez, R., Varela, H., Rancel, N. & Valladares, F.
825 Microvascular pericytes: a review of their morphological and functional
826 characteristics. *Histol Histopathol* **6**, 269-286 (1991).
827 6. Pallone, T.L. & Silldorff, E.P. Pericyte regulation of renal medullary blood flow.
828 *Exp Nephrol* **9**, 165-170 (2001).
829 7. Simon, C., Lickert, H., Götz, M. & Dimou, L. Sox10-iCreERT2 : a mouse line to
830 inducibly trace the neural crest and oligodendrocyte lineage. *Genesis* **50**, 506-
831 515 (2012).
832 8. Etchevers, H.C., Vincent, C., Le Douarin, N.M. & Couly, G.F. The cephalic neural
833 crest provides pericytes and smooth muscle cells to all blood vessels of the face
834 and forebrain. *Development* **128**, 1059-1068 (2001).
835 9. Yu, Q.C., Song, W., Wang, D. & Zeng, Y.A. Identification of blood vascular
836 endothelial stem cells by the expression of protein C receptor. *Cell Res* **26**, 1079-
837 1098 (2016).

838 10. Wang, Y. *et al.* Ephrin-B2 controls VEGF-induced angiogenesis and
839 lymphangiogenesis. *Nature* **465**, 483-486 (2010).
840 11. Science, A.I.f.B. TECHNICAL WHITE PAPER: TRANSGENIC
841 CHARACTERIZATION. *Allen Brain Atlas* **9** (2015).
842 12. Kilani, B. *et al.* Comparison of endothelial promoter efficiency and specificity in
843 mice reveals a subset of Pdgfb-positive hematopoietic cells. *J Thromb Haemost*
844 **17**, 827-840 (2019).
845 13. Planas, A.M. Role of Immune Cells Migrating to the Ischemic Brain. *Stroke* **49**,
846 2261-2267 (2018).
847 14. Fernandez-Klett, F. *et al.* Early loss of pericytes and perivascular stromal cell-
848 induced scar formation after stroke. *J Cereb Blood Flow Metab* **33**, 428-439
849 (2013).
850 15. Pu W, et al. Genetic Targeting of Organ-Specific Blood Vessels. Circ Res. 2018
851 Jun 22;123(1):86-99.
852 16. Krolak T, et al. A High-Efficiency AAV for Endothelial Cell Transduction
853 Throughout the Central Nervous System. Nat Cardiovasc Res. 2022
854 Apr;1(4):389-400.
855 17. Piera-Velazquez, S. & Jimenez, S.A. Endothelial to Mesenchymal Transition:
856 Role in Physiology and in the Pathogenesis of Human Diseases. *Physiol Rev* **99**,
857 1281-1324 (2019).
858 18. Hulshoff, M.S., Xu, X., Krenning, G. & Zeisberg, E.M. Epigenetic Regulation of
859 Endothelial-to-Mesenchymal Transition in Chronic Heart Disease. *Arterioscler*
860 *Thromb Vasc Biol* **38**, 1986-1996 (2018).

861 19. Armulik A, et al. Pericytes regulate the blood-brain barrier. Nature. 2010 Nov
862 25;468(7323):557-61. doi: 10.1038/nature09522. Epub 2010 Oct 13. PMID:
863 20944627.

864 20. Daneman R, et al. Pericytes are required for blood-brain barrier integrity during
865 embryogenesis. Nature. 2010 Nov 25;468(7323):562-6.

866 21. Goumans MJ, Mummery C. Functional analysis of the TGFbeta receptor/Smad
867 pathway through gene ablation in mice. Int J Dev Biol. 2000 Apr;44(3):253-65.
868 PMID: 10853822.

869